

SEMI-INSULATING BUFFER LAYER TECHNOLOGY

ANNUAL REPORT FOR THE PERIOD
March 1, 1981 through April 30, 1982

AD A120203

CONTRACT NO. F49620-81-C-0038

Prepared for

Air Force Office of Scientific Research
Electronic and Solid State Sciences
Building 410
Bolling AFB, Washington, DC 20332

R.D. Fairman
Principal Investigator

JULY 1982

DTIC
OCT 12 1982
E

DTIC FILE COPY

Approved for public release; distribution unlimited



Rockwell International

02 10 12 101

UNCLASSIFIED

SECURITY CLASSIFICATION OF THIS PAGE (When Data Entered)

REPORT DOCUMENTATION PAGE		READ INSTRUCTIONS BEFORE COMPLETING FORM
1. REPORT NUMBER AFOSK-TR- 82 - 0861	2. GOVT ACCESSION NO. <i>ADA122 223</i>	3. RECIPIENT'S CATALOG NUMBER
4. TITLE (and Subtitle) Semi-Insulating Buffer Layer Technology	5. TYPE OF REPORT & PERIOD COVERED Annual Report for the period 03/01/81-04/30/82	
	6. PERFORMING ORG. REPORT NUMBER MRDC41086.2ARF	
7. AUTHOR(s) R.D. Fairman and J.R. Oliver	8. CONTRACT OR GRANT NUMBER(s) F49620-81-C-0038	
9. PERFORMING ORGANIZATION NAME AND ADDRESS Rockwell International Microelectronics Research and Development Center, 1049 Camino Dos Rios, Thousand Oaks, California 91360	10. PROGRAM ELEMENT, PROJECT, TASK AREA & WORK UNIT NUMBERS ████████ 2306/B1 <i>61102F</i>	
11. CONTROLLING OFFICE NAME AND ADDRESS Air Force Office of Scientific Research Building 410 Bolling AFB, DC 20332	12. REPORT DATE July 1982	
	13. NUMBER OF PAGES 58	
14. MONITORING AGENCY NAME & ADDRESS (if different from Controlling Office)	15. SECURITY CLASS. (of this report) UNCLASSIFIED	
	15a. DECLASSIFICATION/DOWNGRADING SCHEDULE	
16. DISTRIBUTION STATEMENT (of this Report) Approved for public release; distribution unlimited.		
17. DISTRIBUTION STATEMENT (of the abstract entered in Block 20, if different from Report)		
18. SUPPLEMENTARY NOTES		
19. KEY WORDS (Continue on reverse side if necessary and identify by block number) Epitaxial growth, VPE, AsCl ₃ , Ga, H ₂ Semi-insulating GaAs Buffer layer growth GaAs <i>a</i>		
20. ABSTRACT (Continue on reverse side if necessary and identify by block number) "Semi-insulating buffer layer technology" describes a study of undoped and intentionally doped epitaxial buffer layers grown on lightly chromium doped horizontal Bridgman and undoped LEC substrates. Specific effects of substrate impurity redistribution from bulk substrates are described by improved characterization techniques such as SIMS depth profiling, 4K Photoluminescence, Photo Induced Transient Spectroscopy (PITS) and Spark Source Mass Spectrometry (SSMS). Important correlation of dominant		

DD FORM 1473

1 JAN 73

EDITION OF 1 NOV 65 IS OBSOLETE

UNCLASSIFIED

SECURITY CLASSIFICATION OF THIS PAGE (When Data Entered)

UNCLASSIFIED

SECURITY CLASSIFICATION OF THIS PAGE(When Data Entered)

Impurity centers has been established by Dark Conductivity Measurements.

An important discovery of Fe redistribution in epitaxial layers during vapor phase growth was made by detailed chemical, optical and electrical transport measurements on undoped epitaxial layers.

An assessment of the effects of Oxygen doping in VPE GaAs was made using $^{18}O_2$ which resulted in the identification of an O_2 -related deep donor at $E_c - 0.67$ eV. P-type conductivity resulting from O_2 doping was shown to be due to a dominant Fe^{2+} center. Effects of carrier removal by O_2 doping were also shown.

80/2

024301

UNCLASSIFIED

SECURITY CLASSIFICATION OF THIS PAGE(When Data Entered)



TABLE OF CONTENTS

	<u>Page</u>
1.0 INTRODUCTION.....	1
2.0 TECHNICAL DISCUSSION.....	3
2.1 Review of Vapor Phase Epitaxy.....	3
2.2 Present AsCl ₃ VPE Technology.....	8
2.3 Epitaxial Growth Procedure.....	10
2.4 Accomplishments.....	11
2.4.1 Intrinsic Buffer Layers	11
2.4.2 Chromium Doped Buffer Layers.....	24
2.4.3 Iron Doped Buffer Layers	29
2.4.4 Oxygen Doped Buffer Layers	36
2.4.5 Summary of Progress to Date.....	48
2.5 Recommendations.....	51
3.0 REFERENCES.....	56

Accession For	
NTIS GRA&I	<input checked="" type="checkbox"/>
DTIC TAB	<input type="checkbox"/>
Unannounced	<input type="checkbox"/>
Justification	
By	
Distribution/	
Availability Codes	
and/or	
Distribution	
A	



AIR FORCE OFFICE OF SCIENTIFIC RESEARCH (AFSC)
NOTICE OF TRANSMITTAL TO DTIC

This technical report has been reviewed and is approved for public release IAW AFR 190-12. Distribution is unlimited.

MATTHEW J. KERPER
Chief, Technical Information Division

LIST OF FIGURES

<u>Figure</u>		<u>Page</u>
1	Hall Mobility versus net carrier concentration.....	4
2	Gallium to arsenic ratio versus mole fraction of AsCl_3 in H_2	6
3	Schematic of epitaxial reactor.....	7
4	Vapor phase epitaxial reactor photo.....	9
5	Surface morphology, undoped VPE buffer layers.....	12
6	Block diagram of PITS instrumentation.....	14
7	Normalized photo induced transient spectroscopy, undoped and Cr doped VPE buffers.....	15
8	Activation energy, undoped VPE buffer.....	17
9	SIMS depth profile, undoped VPE buffer layer.....	19
10	4K photoluminescence spectra, Fe in GaAs.....	20
11	1.2K photoluminescence spectra, residual acceptors in VPE GaAs.....	21
12	VPE donor and acceptor concentration versus AsCl_3 mole fraction.....	23
13	Carrier profiles of active layers grown on VPE Cr doped buffers.....	26
14	SIMS depth profile, Cr doped VPE buffer layer.....	27
15	Normalized photo induced transient spectroscopy, undoped and Cr doped VPE buffers.....	28
16	Activation energy, Cr doped VPE buffer.....	30
17	SIMS depth profile, Fe doped VPE buffer layer.....	32
18	Normalized photo induced transient spectroscopy, Cr doped bulk GaAs.....	33
19	4K photoluminescence spectra, Fe in GaAs.....	34



LIST OF FIGURES (continued)

	<u>Page</u>
20 4K photoluminescence, Fe ²⁺ versus SIMS concentration, VPE GaAs.....	35
21 Normalized PITS spectrum, Fe doped buffer.....	37
22 Activation energy, Fe doped buffer.....	38
23 Surface morphology, oxygen doped VPE buffer.....	39
24 Resistivity of O ₂ doped VPE buffer versus O ₂ concentration.....	41
25 SIMS depth profile, ¹⁸ O ₂ doped VPE buffer 1375.....	43
26 SIMS depth profile, ¹⁸ O ₂ doped VPE buffer 1377.....	44
27 Verification of ¹⁸ O ₂ dopant by mass spectrometry.....	45
28 Normalized PITS spectrum, ¹⁸ O ₂ doped buffer.....	46
29 Activation energy, ¹⁸ O ₂ doped buffer.....	47
30 Energy level diagram, VPE buffer summary.....	52



Rockwell International

MRDC41086.2ARF

PREFACE

This work was conducted in the Microwave Devices Section of the Gallium Arsenide Electronic Device Research department at the Rockwell International Microelectronic Research and Development Center, Thousand Oaks, California. Personnel contributing to this effort include Mr. Robert D. Fairman, Mr. John R. Oliver (materials growth and characterization) and Dr. Herbert Kroemer (consultant) University of California, Santa Barbara assisting in the interpretation of data and impurity modeling.

The principle investigator was Mr. Robert D. Fairman. This work is sponsored by the Air Force Office of Scientific Research under contract F49620-81-C0038 and monitored by Dr. Gerald L. Witt, program manager, Air Force Office of Scientific Research, Bolling AFB, DC.



1.0 INTRODUCTION

The significance of semi-insulating Gallium Arsenide has never been more critical for the fabrication of high performance MESFET devices than it is today. The emergence of a high technology GaAs requirement now reaches to 40 GHz. Direct ion implantation into bulk semi insulating substrates has shown great promise in the circuit integration area. Many of the highly complex digital logic and memory circuits are now and will be fabricated by direct ion implantation in the future.

It is apparent however that other devices, especially in the microwave area may benefit from higher purity epitaxial layers for low noise and/or high power applications. Epitaxial technology has been the mainstay of low noise and high power devices at the present state of the art. The future high frequency (>30 GHz) satellite and secure telecommunications systems may depend upon this well developed technology.

The ever increasing demand for high purity, high resistivity epitaxial buffer layers will continue with the need for increased device performance and high frequency capability. Device problems associated with back-gating, high noise levels and impurity transport need certainly to be addressed. Needs for not only improved semi-insulating buffer layers but for well understood, reproducible processes are now critical.

Past progress in epitaxial materials technology has been restricted by a limited understanding and identification of the deep impurity centers present and means for their control. Characterization methods for semi-insulating GaAs have not been well developed nor highly specific for identification of deep impurity centers until just recently. Application of a newly developed trap analysis technique, Photo Induced Transient Spectroscopy, has allowed great progress to be made in understanding the major deep impurity centers in semi-insulating GaAs.



Initial efforts in this program have been successful in providing a number of representative samples with specific, intentional deep impurities for study and further characterization. Excellent examples of impurity diffusion from commercial, semi-insulating substrates have been observed by analysis performed both at Rockwell and AFWAL to provide definitive data and concise identification of cause and effect. As a result higher purity undoped buffer layers have also been grown demonstrating the value of these diagnostic studies. Investigation of the controversial effects of O_2 in VPE GaAs have been initiated and several important pieces of data have already been obtained. Oxygen continues to be one of the most important contaminants in GaAs growth and is the least understood to date. Using specific tracer techniques in this program it has been shown that oxygen has extremely limited solubility in VPE GaAs. The resultant changes in the electronic properties of VPE GaAs due to " O_2 doping" are presently being studied with 4K Photoluminescence and Photo Induced Transient Spectroscopy.



2.0 TECHNICAL DISCUSSION

2.1 Review of Vapor Phase Epitaxy

The major objective in this program is to study the principle types of semi-insulating GaAs buffer layers now in use and provide an in-depth analysis of their fundamental properties and problems in application to GaAs MESFET devices. Analysis of the vapor transport process will be performed and modifications made only to perfect specific types of buffer layers under study. The advanced characterization techniques used in this program will permit the identification and resolution of impurities limiting performance of high frequency microwave devices.

The epitaxial process proposed for this program was selected on the basis of:

- 1) Highest known purity (Fig. 1)
- 2) Demonstrated most useful in present buffer layer and multilayer growth
- 3) Basic process with fewest variables for research study
- 4) State of the art capabilities for program are available at Rockwell - MRDC.

The $\text{AsCl}_3, \text{Ga}, \text{H}_2$ process was selected because of its inherent simplicity in performing high purity epitaxy with the fewest chemical variables. The key features of the process are:

I. High Purity Aspects

- a) Performs a direct synthesis of GaAs and epitaxial growth by vapor transport.
- b) All chemical agents and elements are of the best available purity (7-9s) with excellent availability.
- c) Epitaxy process incorporates two purification mechanisms
 - 1) Segregation of n and p type impurities in Ga/GaAs source. GaAs crust forms by a solution growth method producing a very pure GaAs source for transport.



MRDC82-16092

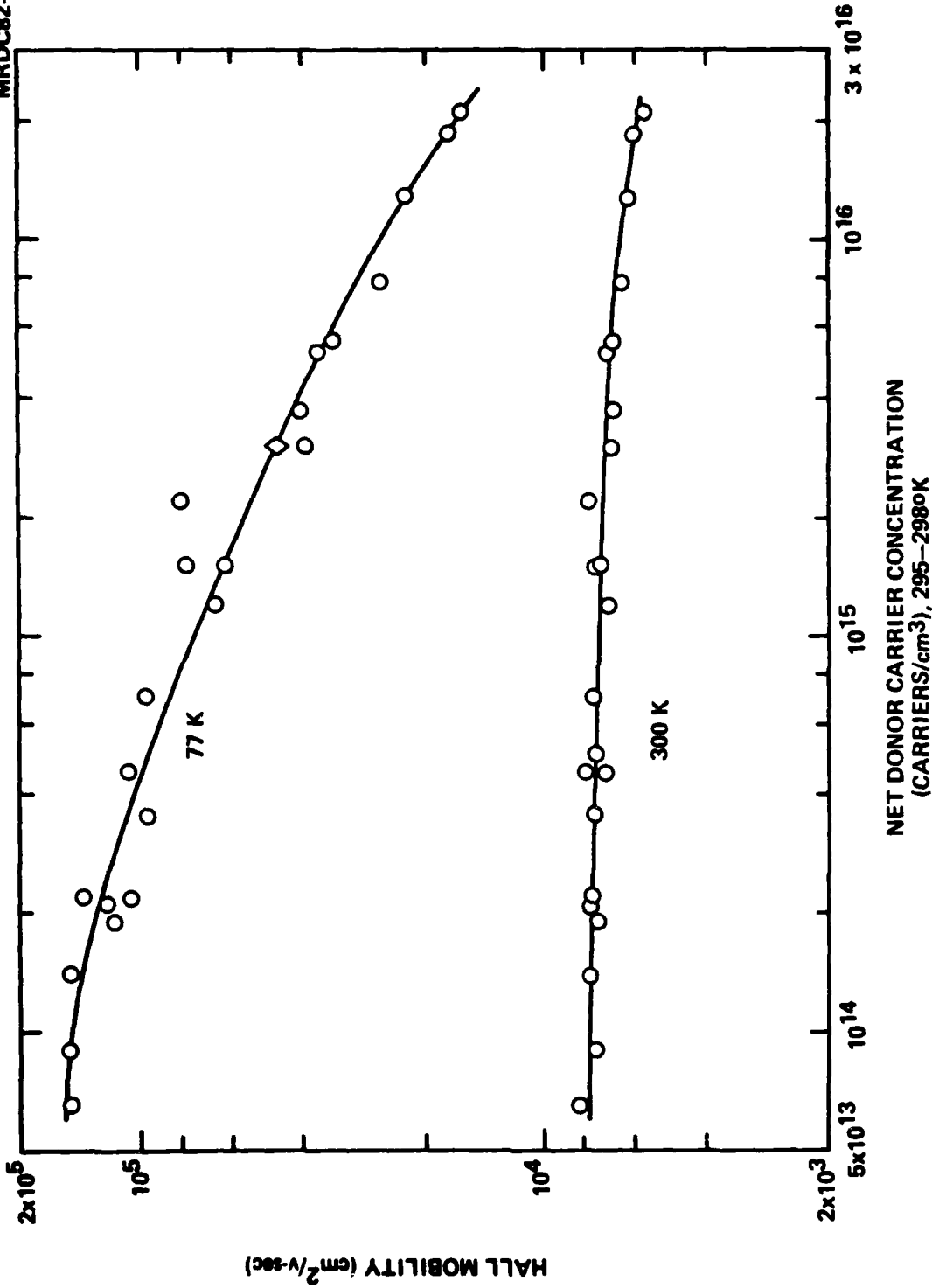


Fig. 1 Hall Mobility vs. Net Donor Carrier Concentration.



- d) Control mechanisms for minimizing auto doping effects from substrate are well developed.
- e) Reactors and construction (spectrographic grade fused silica) is purest available for semi conductor processing.
- f) Transport medium (H_2) easily purified to extremely high purity.

II. Stoichiometry

- a) Ga/As ratio control subject to one variable in first order ($AsCl_3$ temp and furnace temp)
- b) Gas flow rates are not critical for Ga/As control
- c) Stoichiometry fixed near optimum (2:1) point with fine control over a 30% range (Fig. 2).

III. Multilayer Capabilities

- a) Multilayer growth with controlled doping and carrier profile easily attained
- b) p/n junction growth established
- c) Excellent control over autodoping between multi-layers
- d) High purity buffer layer growth established in 1968.
- e) Control of epitaxy and vapor etching easily performed with use of HCl for substrate etching and in-process alteration of purity and growth rate.

Separate $AsCl_3$ sources are provided to perform the following modes of growth: 1) Ga transport, 2) substrate in-situ, etching, 3) Transport of refractory metal dopants (Cr, Fe), 4) Impurity reduction via xs HCl over-pressure effects as shown in Fig. 3.

Provisions have been made to add gaseous dopant sources (H_2S , H_2Se , SiH_4) with gas blending to control doping concentrations over three orders of magnitude.



MRDC 82-16176

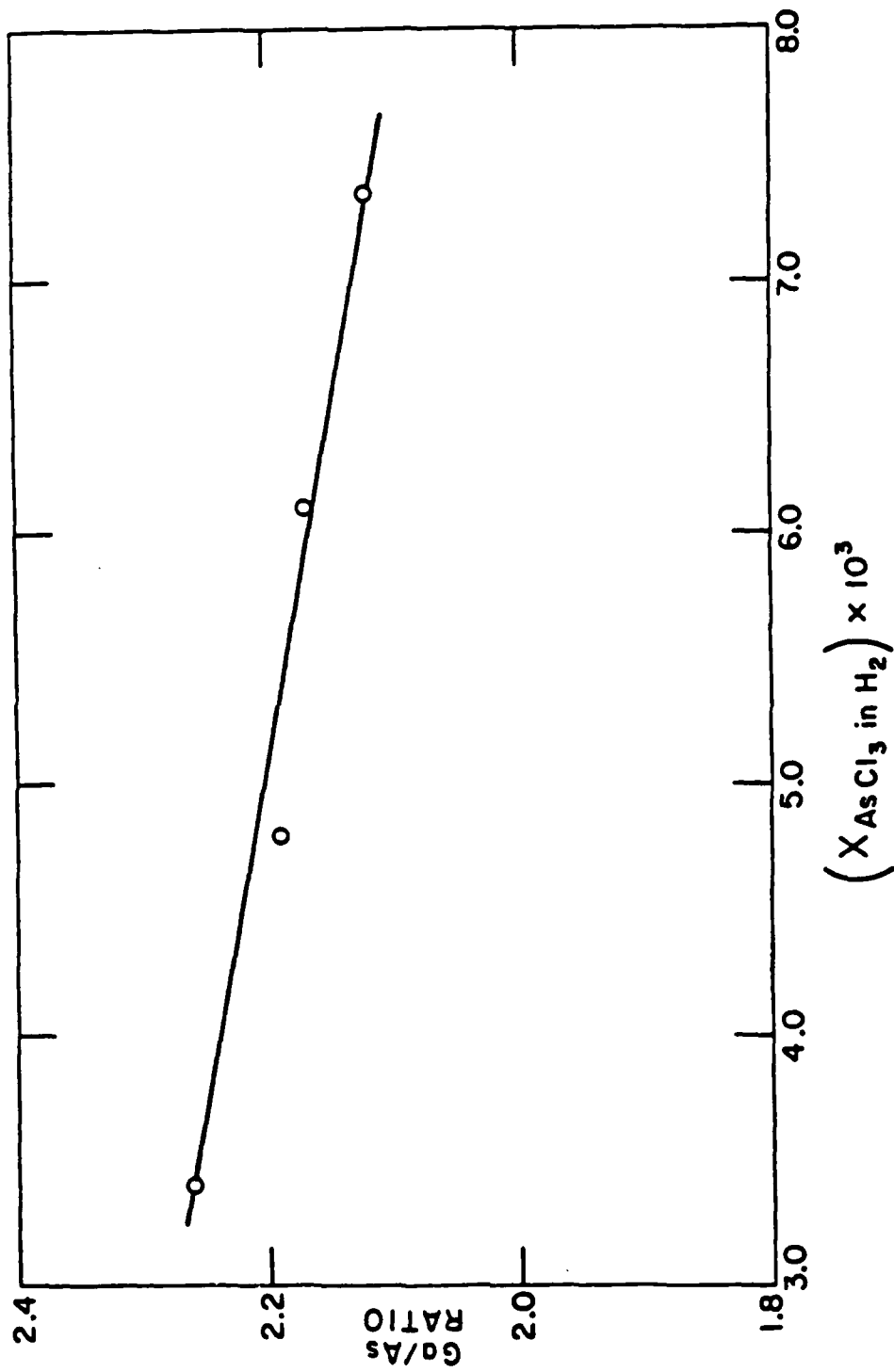
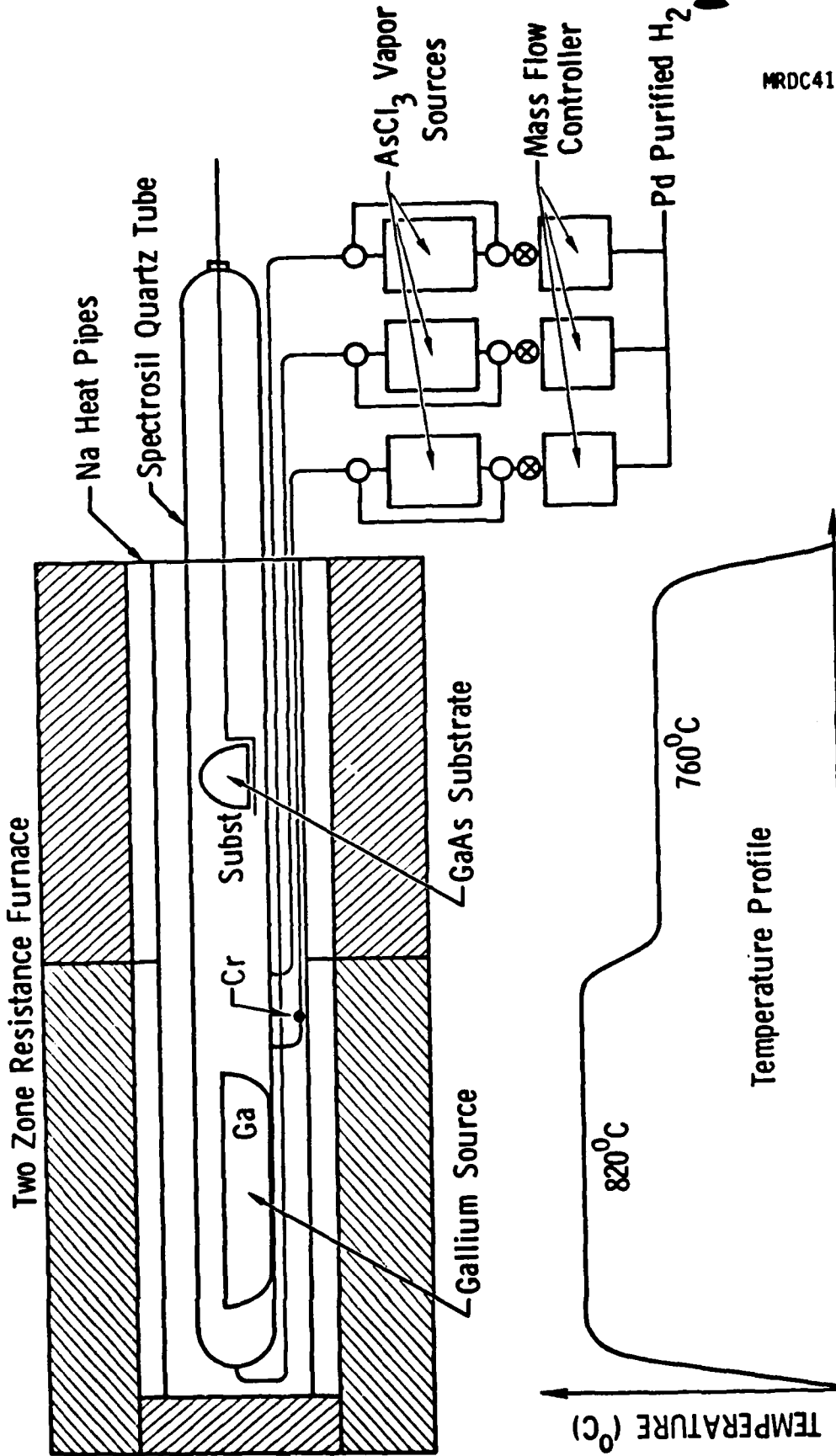


Fig. 2 Gallium to arsenic ratio versus mole fraction of AsCl₃ in H₂. (F33615-68-C-1136)

SC78-2084A



Rockwell International

MRDC41086.2ARF

Fig. 3 Schematic of Epitaxial reactor.



Rockwell International

MRDC41086.2ARF

MRDC82-17587

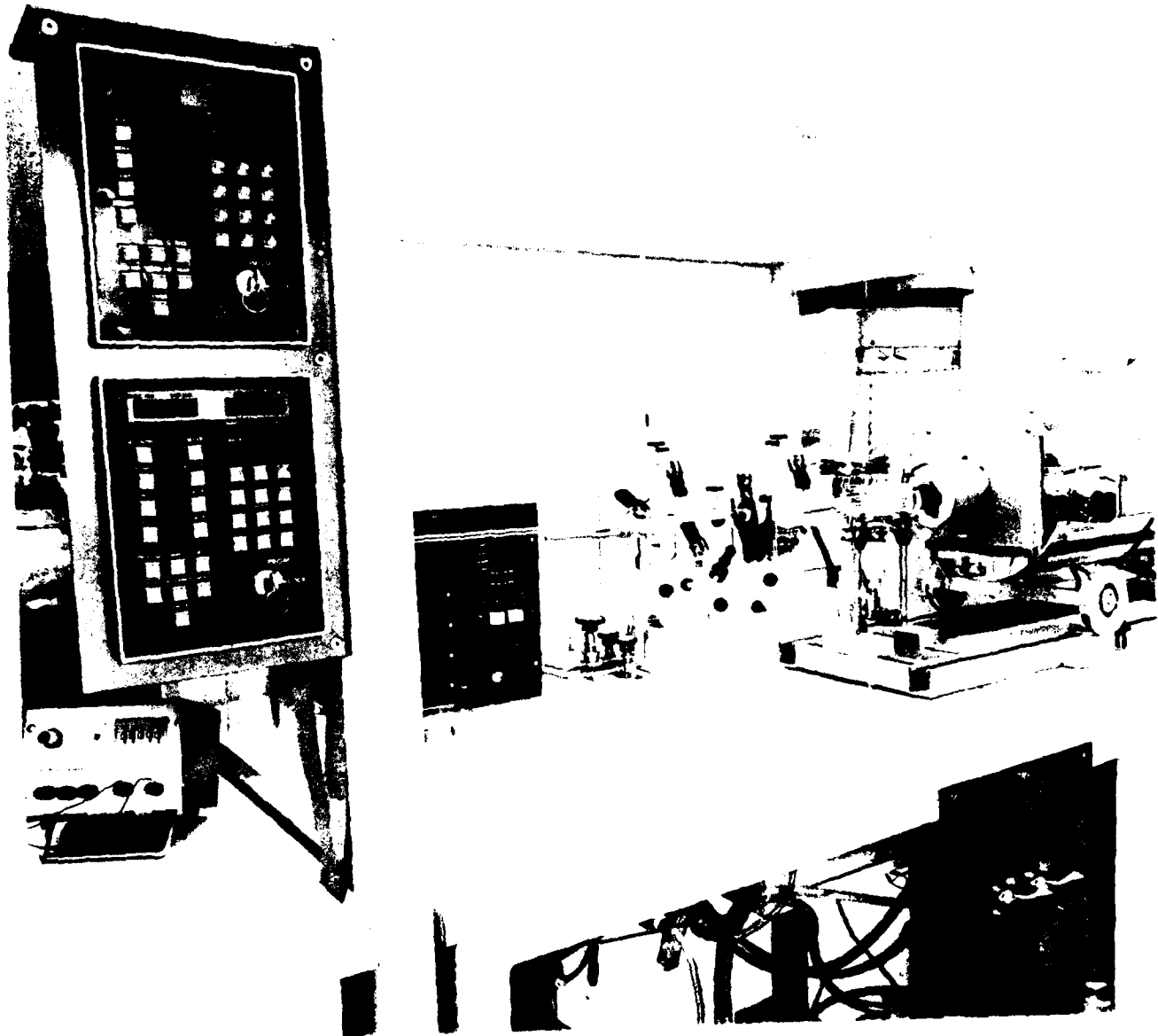


Fig. 4 Vapor phase epitaxial reactor system.



The reactor can be brought to rapid thermal equilibrium with the rolling, preheated furnace equipped with Na filled heat pipes to provide an extremely uniform thermal geometry for vapor transport and epitaxial growth.² The reactor tube is constructed from Spectrosil fused silica to reduce exposure to the metallic impurity oxides of Fe, Mg, Ca and Ti found in laboratory grade silica. All aspects of the reactor have been studied carefully over the past ten years to provide extremely laminar gas flow for a uniform deposition regime. A careful compromise between the Gallium source and substrate deposition temperature were determined to both limit the activity of Si in the Ga source due to solubility and reduce the net deposition rate to that useful in producing submicron thick layers.³ Extensive studies of auto doping have been conducted in the past to allow growth to clean well ordered substrate/epitaxial layer interfaces with minimum contributions from substrate dopants.

2.3 Epitaxial Growth Procedure

The epitaxial reactor is prepared by first determining the leak integrity with a vacuum - Helium leak detector to $< 10^{-9}$ cc/sec. High temperature baking in H_2 (850°C) is performed to remove absorbed moisture.

The gallium (7-9's) is also baked out but at a lower temperature (820°C) for 12 hours prior to saturation with As. Removal of residual moisture is important in assuring high carrier mobilities, free of compensating effects.

Following As saturation by transport of $AsCl_3:H_2$ mixtures the reactor is ready for use in epitaxial growth. The operation sequence for epitaxial growth is outlined below:

- a) Sample loading and purging
- b) Thermal equilibration to operating temperature
- c) GaAs source saturation, vapor etching of sample
- d) Initiation of epitaxial growth/termination of growth
- e) Removal of furnace/cool to room temperature/unload.



Modifications to the above procedure are made to incorporate dopants via gas phase by use of solid sources (Cr,Fe) or gas mixtures (H_2S, SiH_4).

2.4 Accomplishments

The primary task during the first phase of this program was that of screening for symptomatic, first order problems in each particular buffer layer category. Data obtained reveals many present day difficulties that may now be either avoided entirely or easily resolved in future work due to the focus of this study.

A review of each category will be made with complete details of preparation and preliminary characterization updated to the present phase of this work.

2.4.1 Intrinsic Buffer Layers:

Preparation Data: Doping: No intentional dopant used

Arsenic Trichloride mole Fraction: $9-11 \times 10^{-3}$

AsCl₃: Mitsubishi Lot #6425, 7-9's

Gallium Source: Eagle Picher R-651K, 7-9's purity

T_{source}: 820°C

T_{substrate}: 760°C

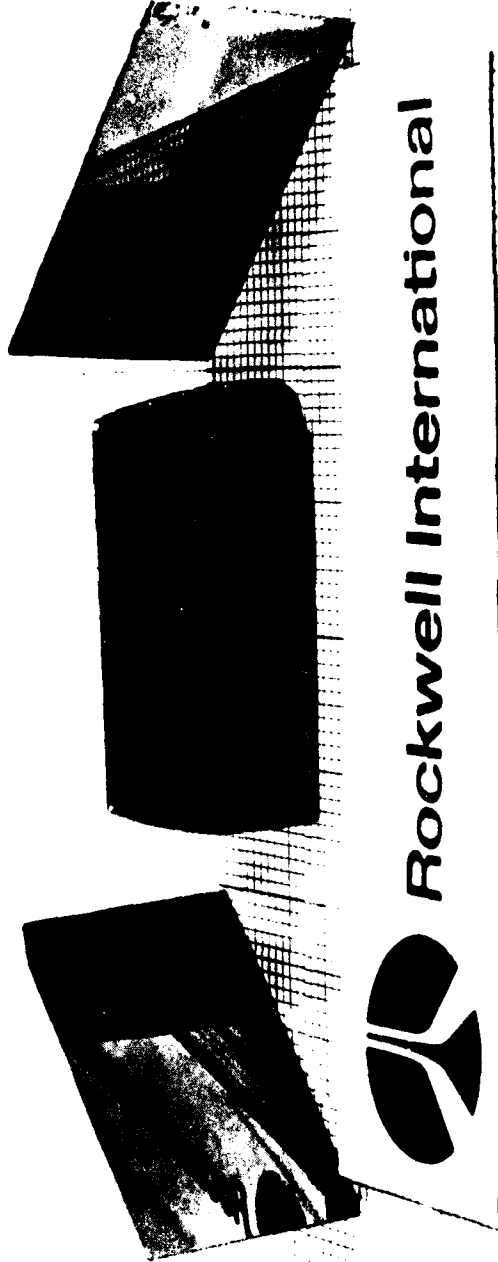
Flowrate: GaAs Transport (330 sccm)

Substrate: Cr doped Horizontal Bridgman (HB) and undoped LEC

Evaluation

Morphology: Smooth well ordered layers with slight surface texture as shown Fig. 5.

MRDC82-17588



Rockwell International

MRDC41086.2ARF

Fig. 5 Surface morphology, undoped VPE buffer layers.

Routine Electrical Data

<u>Sample</u>	<u>Type</u>	<u>Approx. Net Doping</u>	<u>Layer Thickness</u>	<u>Substrate</u>	<u>$\chi_{\text{AsCl}_3} \times 10^3$</u>
1352	p-	$<10^{13} \text{ cm}^{-3}$	21 μm	R7/C ⁽¹⁾	11.8
1349	p-	$<10^{13} \text{ cm}^{-3}$	35 μm	$\chi\text{S-254}^{(2)}$	11.8
1361	p-	$\ll 10^{13} \text{ cm}^{-3}$	40 μm	C3-28 ⁽¹⁾	10.1
1381	n	$\sim 10^{14} \text{ cm}^{-3}$	24 μm	C3-28	9.0
1362	p-	$\ll 10^{13} \text{ cm}^{-3}$	5 μm	G-22-14J ⁽²⁾	10.6

(1) Undoped LEC substrates

(2) Cr doped Horizontal Bridgman Substrates

Electrical Transport Measurement

Trap energies and emission rates were determined by the photo-induced transient spectroscopy technique or PITS. We prefer this nomenclature over optical-DLTS, since the latter historically refers to capacitance transients in a depletion region, whereas in PITS we are dealing with the rise or decay of photo current. The spectrum is obtained in the usual manner by sampling either the rise (R-PITS) or decay (D-PITS) of the photo current at two points in time, with the difference $\Delta I = I_1 - I_2 = I_{\text{SIG}}$ recorded continuously as a function of temperature. Any peaks observed in the spectrum will correspond to a trap emission rate which is directly proportional to the sampling frequency; successive scans at different frequencies will therefore determine both the trap energy and capture cross section, assuming a single-exponential rise or decay. These spectra were recorded using chopped monochromatic light, with the resulting photo current amplified by a high-speed pre-amplifier (PAR 181). The pre-amplifier output is fed into a sample/hold amplifier followed by a synchronous (lock-in) detector as shown in Fig. 6. The sampling time constant can be varied from 0.27-18 ms, and the temperature from 60-450°K. Thus, all except the very shallow traps ($<0.1 \text{ eV}$) can be observed with this apparatus.

The spectra presented in Fig. 7 are representative of the samples examined. Epilayer data were obtained with two ohmic contacts spaced 5 μm



PITS INSTRUMENTATION

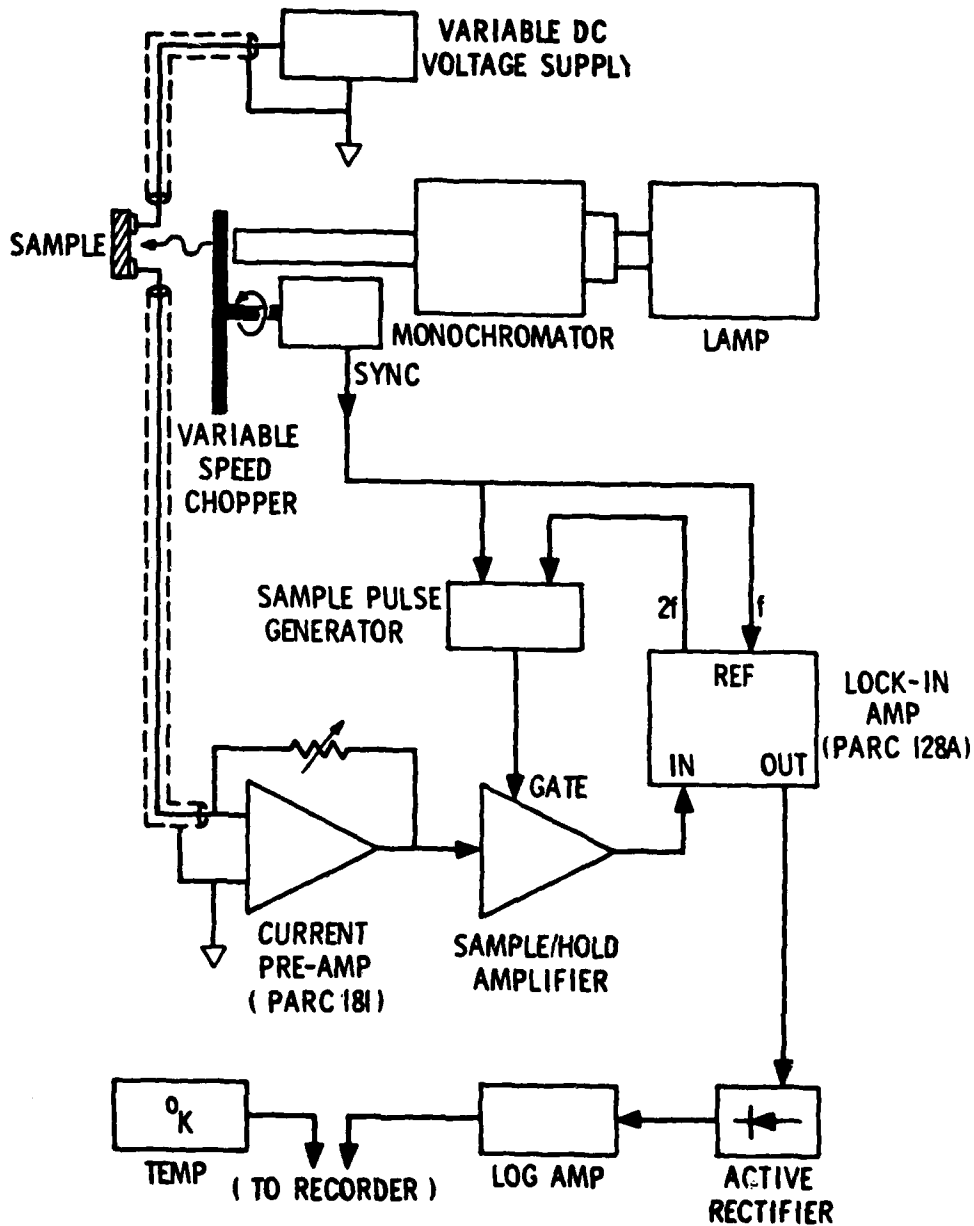


Fig. 6 Block diagram of PITS instrumentation.

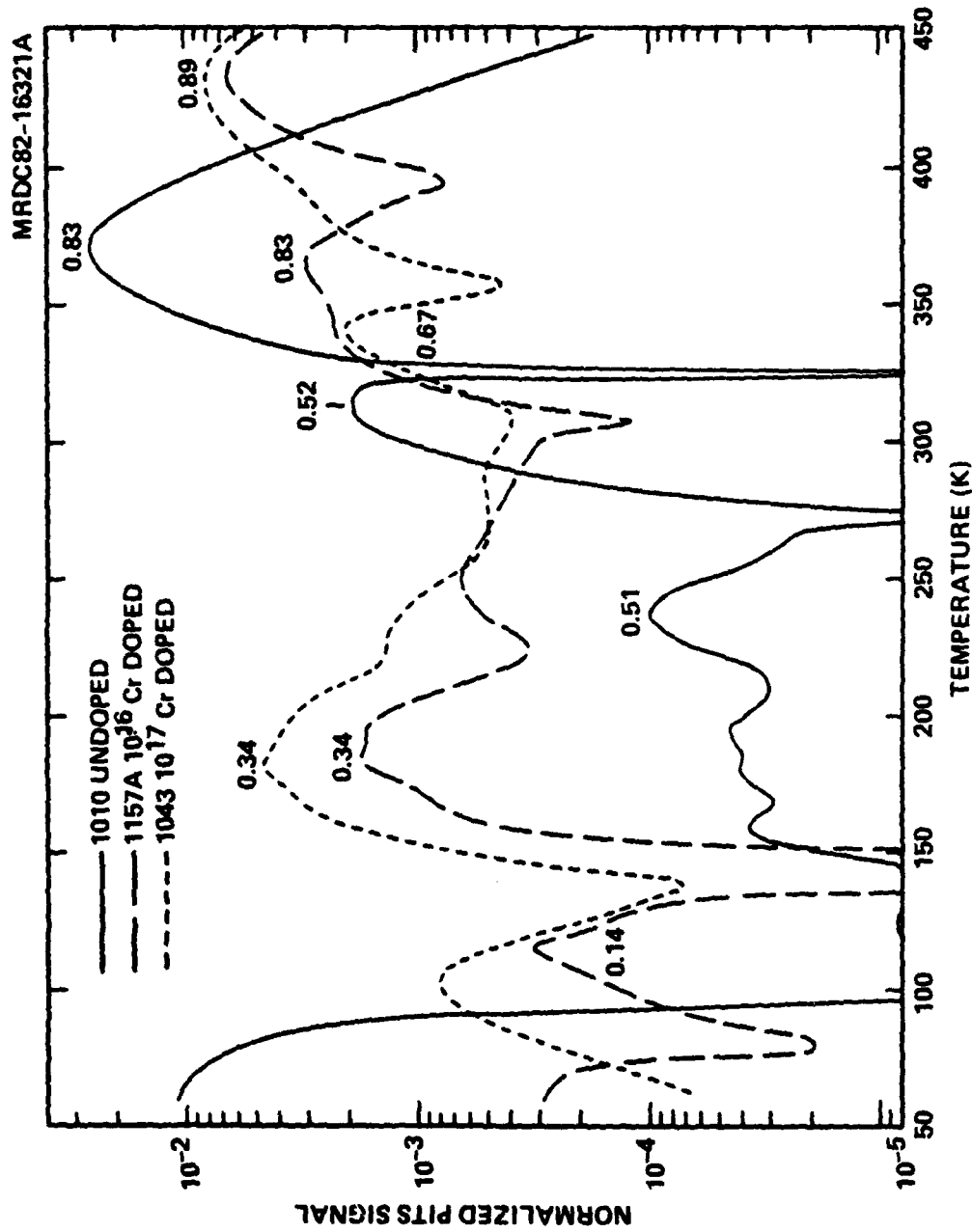


Fig. 7 Normalized photo induced transient spectroscopy, undoped and Cr doped VPE buffers.



apart on the epilayer surface and slightly greater than bandgap (1.55 eV) photon energy. DC bias voltages were held to moderate levels in order to prevent any high-field current injection.

The magnitude of a particular peak is a function of the trap emission rate, free carrier lifetime, the degree of trap filling, and trap concentration. A numerical analysis of trap concentrations is beyond the present scope of this work. However, qualitative comparisons of various traps can be made when the peak heights are normalized by the steady state photo current.

The PITS measurement allows a very complete assessment of both hole and electron traps to be obtained, however, this data requires correlation with a Fermi level measurement to determine the dominant center controlling conductivity. A measurement of dark current vs temperature is made and displayed as an Arrhenius plot of conductivity vs temperature. The slope of the curve provides an activation energy that correlates well with the dominant centers determined by PITS. This activation energy measurement with closely spaced contacts permits an unambiguous determination of the dominant center. Other methods such as Hall vs temperature are performed with macrosamples where interface and substrate currents affect the accuracy required to identify the controlling center in high resistivity layers. PITS spectra of undoped and Cr doped VPE shown in Fig. 7 illustrates the lower trap concentrations observed in the epitaxial layers compared to those observed in the Cr doped Horizontal Bridgman and LEC substrates shown in Fig. 17. Undoped sample 1010 shows the presence of deep native acceptor at $E_v + 0.83$ eV (HL-10), an acceptor at $E_v + 0.52$ eV due to Fe^{2+} , an unidentified electron trap EL-4 at $E_c - 0.51$ eV and some shallow electron traps at <0.1 eV. The entire envelope of trapping centers for undoped VPE 1010 is low compared to the Cr doped buffers and bulk substrates shown in Fig. 7. A dominant electron trap EL-2, $E_c - 0.74$ eV was measured by DLTS at a concentration of $5 \times 10^{15} \text{ cm}^{-3}$. The dominant center controlling resistivity is EL-2 as demonstrated by the activation energy for 1010 shown in Fig. 8.

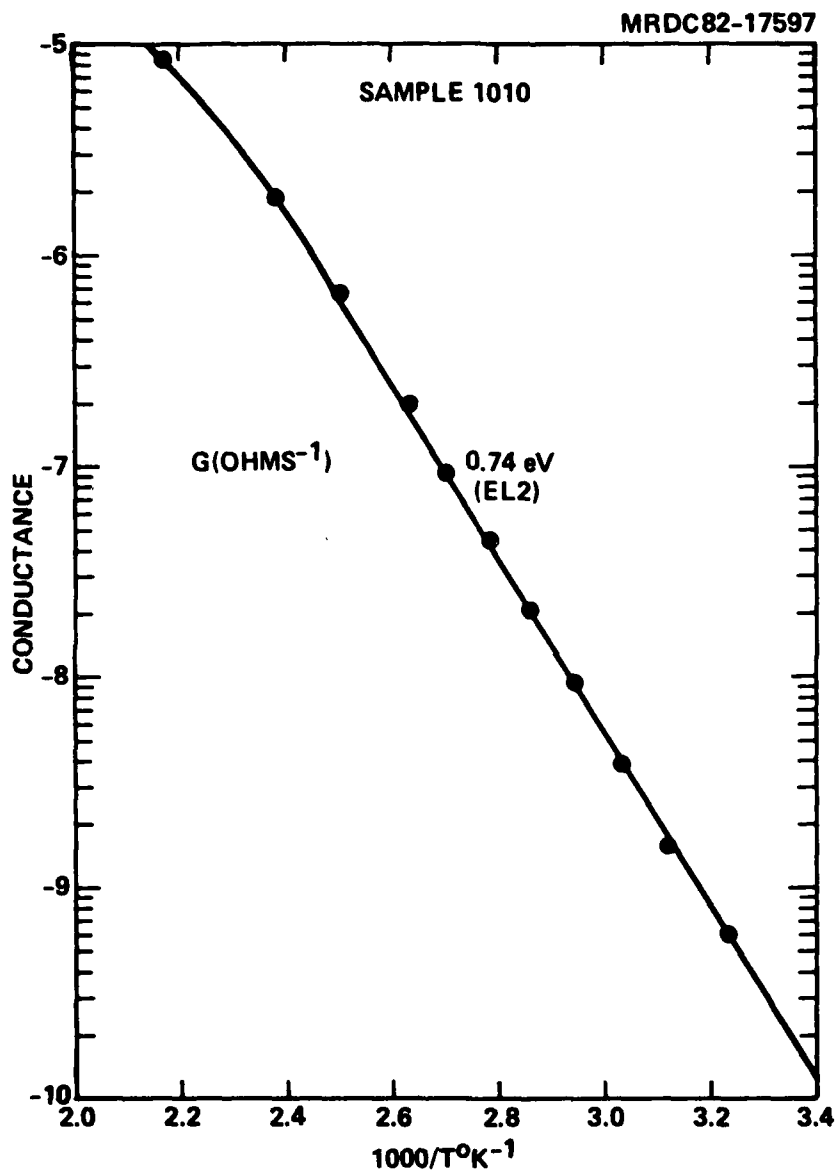


Fig. 8 Activation energy, undoped VPE buffer.



Discussion

High purity undoped buffer layers grown by the AsCl_3 technique can produce isolation from the substrate used. Chemical analysis of the epitaxial layers are shown in Fig. 9 for this analysis of Cr, Fe, Mn, and Mg. The abrupt interface is delineated by the Cr profile in Fig. 9. The resultant carrier type in undoped buffers is very easily influenced by factors other than the VPE process, such as impurity contribution from the semi-insulating substrate. Undoped VPE samples 1349 and 1362 are p type due to the diffusion of Fe from the semi-insulating substrate. Photoluminescence measurements made at Wright-Patterson AFB, Electronics Research Branch⁴ confirmed the presence of Fe in both the epitaxial layers and parent substrate, separately (Fig. 10). Measurements of Cr doped semi-insulating substrates by Photo Induced Transient Spectroscopy or by low temperature photoluminescence have confirmed Fe as a contaminant in all Cr doped semi-insulating GaAs, be it grown by Horizontal Bridgman or LEC⁵ (Fig. 17.) Analysis of high purity chromium metal (Spectrographic grade 6-9's) revealed the following:

<u>Source</u>	<u>Analysis</u>	<u>Application</u>
Johnson Matthey (Spec Pure)	6 ppm Fe	VPE Cr doping
Metals Research (Special Purity)	2 ppm Fe	Bulk Crystal Growth

*Performed at Eagle Picher Inc., AA technique

In the absence of substrate effects the residual carrier type is usually n type as shown in samples 1361 and 1381 with the compensation being determined by two major deep levels located at $E_c - 0.74\text{eV}$ (EL-2) and $E_v + 0.83\text{eV}$ (HL-10). The 0.83 eV hole trap has been observed in both undoped VPE and undoped LEC GaAs.^(6,7) The 0.74 eV electron trap (EL-2) was measured by DLTS. High resolution photoluminescence performed at Electronics Research Lab, WPAFB⁴ indicates the presence of two shallow acceptors Zn and Ge in VPE samples grown on Cr doped substrates E-254 (Fig. 11).



*1374

MRDC82-16313

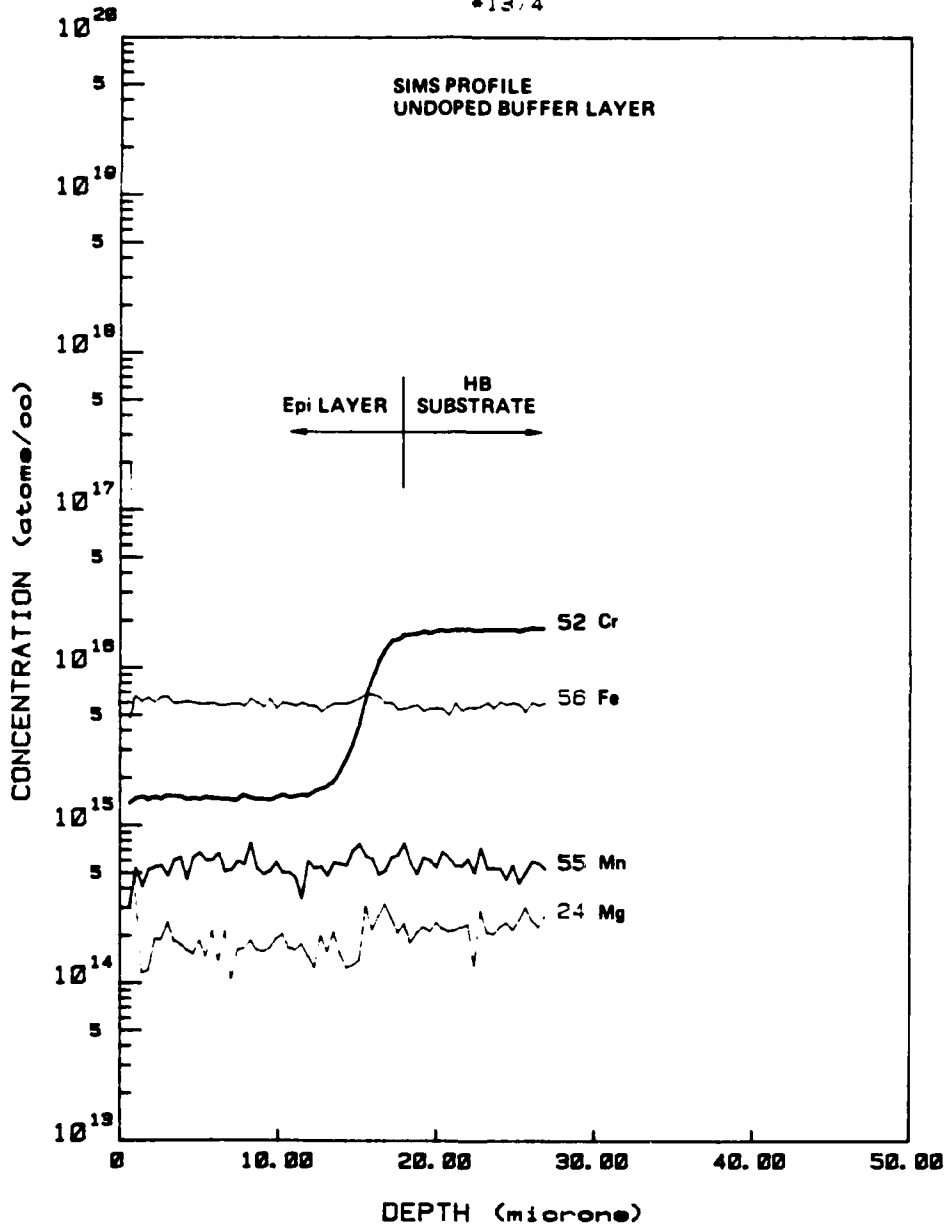


Fig. 9 SIMS depth profile, undoped VPE buffer layer.



MRDC82-16299

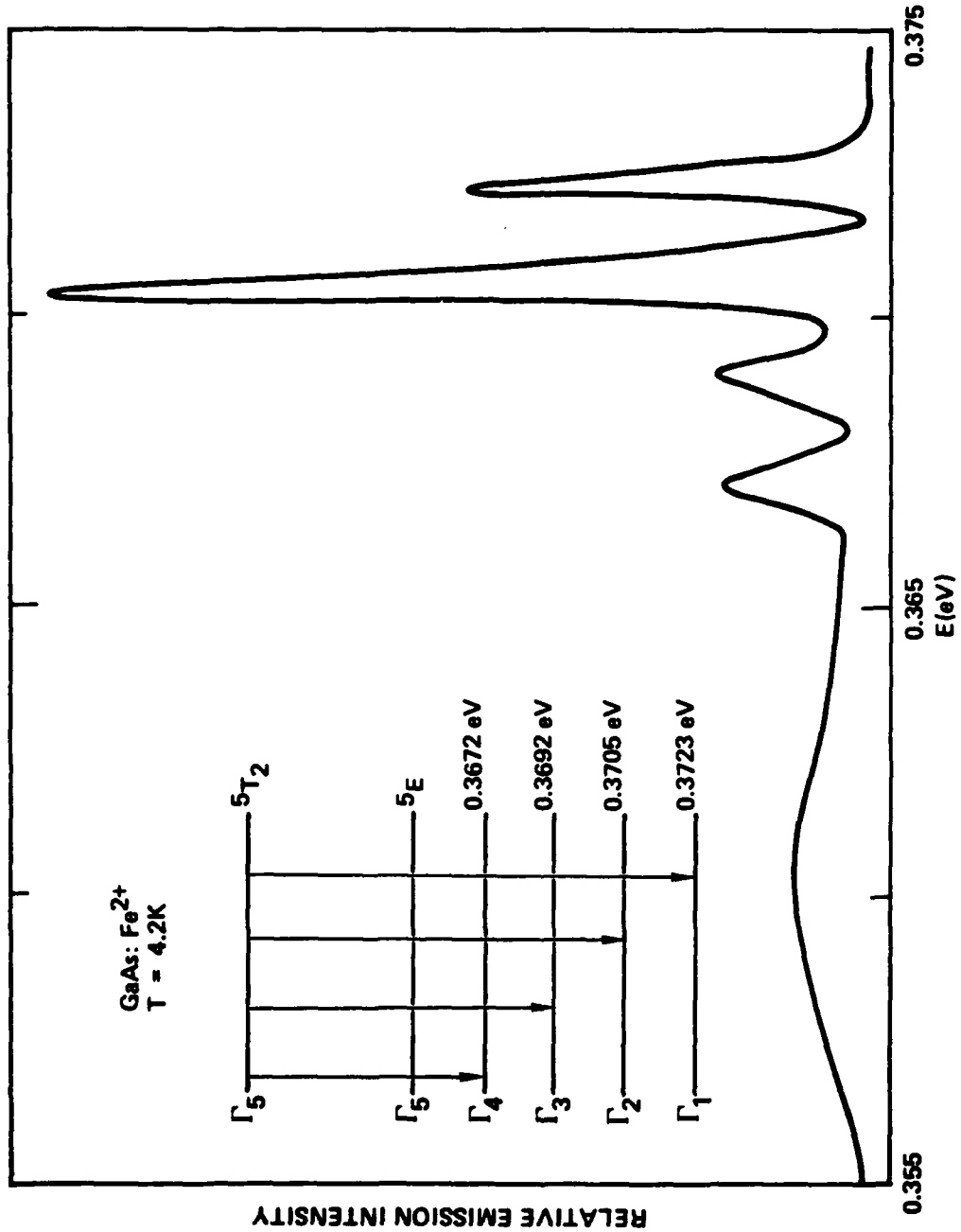


Fig. 10 4K photoluminescence spectra, Fe in GaAs.

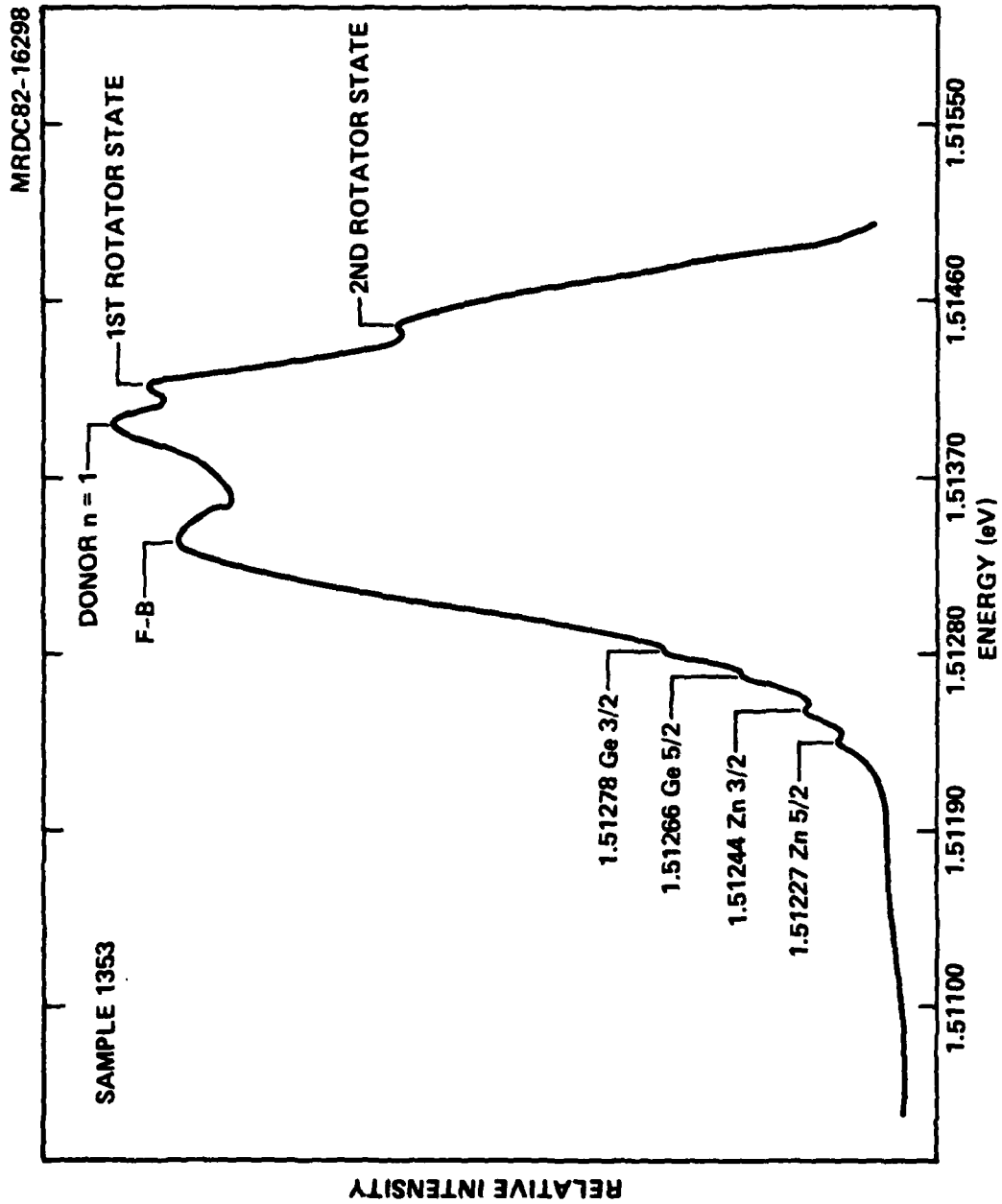


Fig. 11 1.2K photoluminescence spectra, residual acceptors in VPE GaAs.



Those samples grown on high purity undoped LEC substrates do not show shallow acceptor luminescence and are n type with higher resistivity. The resultant carrier type present in the high resistivity VPE buffer layers is controlled by three major factors:

- 1) AsCl_3 mole fraction used (extent of Si suppression)
- 2) Residual acceptor background of reactor and substrate
- 3) Deep levels present (Transition metal impurities and defects)

The thermodynamic control of Si incorporation by the AsCl_3 effect suppresses donors (Si) more strongly than acceptors as shown in Fig. 12. As the AsCl_3 mole fraction approaches 10^{-2} mf, the N_D/N_A ratio approaches 1.0. The resulting carrier type at 10^{-2} mf is highly dependent upon the impurity contribution from the substrate and the relative contribution of residual deep centers (Cr, Fe, EL-2, HL-10).

P type epitaxial layers have all demonstrated inferior electron mobilities ($<300 \text{ cm}^2/\text{V-sec}$) and lower resistivities respective of Fe contamination. Recombination from dominant acceptor centers can act as a noise source in low noise MESFETS. For power FET operation a high resistivity layer is required to tolerate the high electric fields generated by high drain bias voltages which can otherwise cause hole injection in the buffer. Trapped hole charge can give rise to enhanced electron current in the buffer causing a runaway current condition. To resolve the problem of low resistivity p-type layers ($10^4 \Omega\text{cm}$) either high purity semi-insulating substrates with $<2 \times 10^{15} \text{ cm}^{-3}$ Fe must be obtained or light Cr doping must be employed.

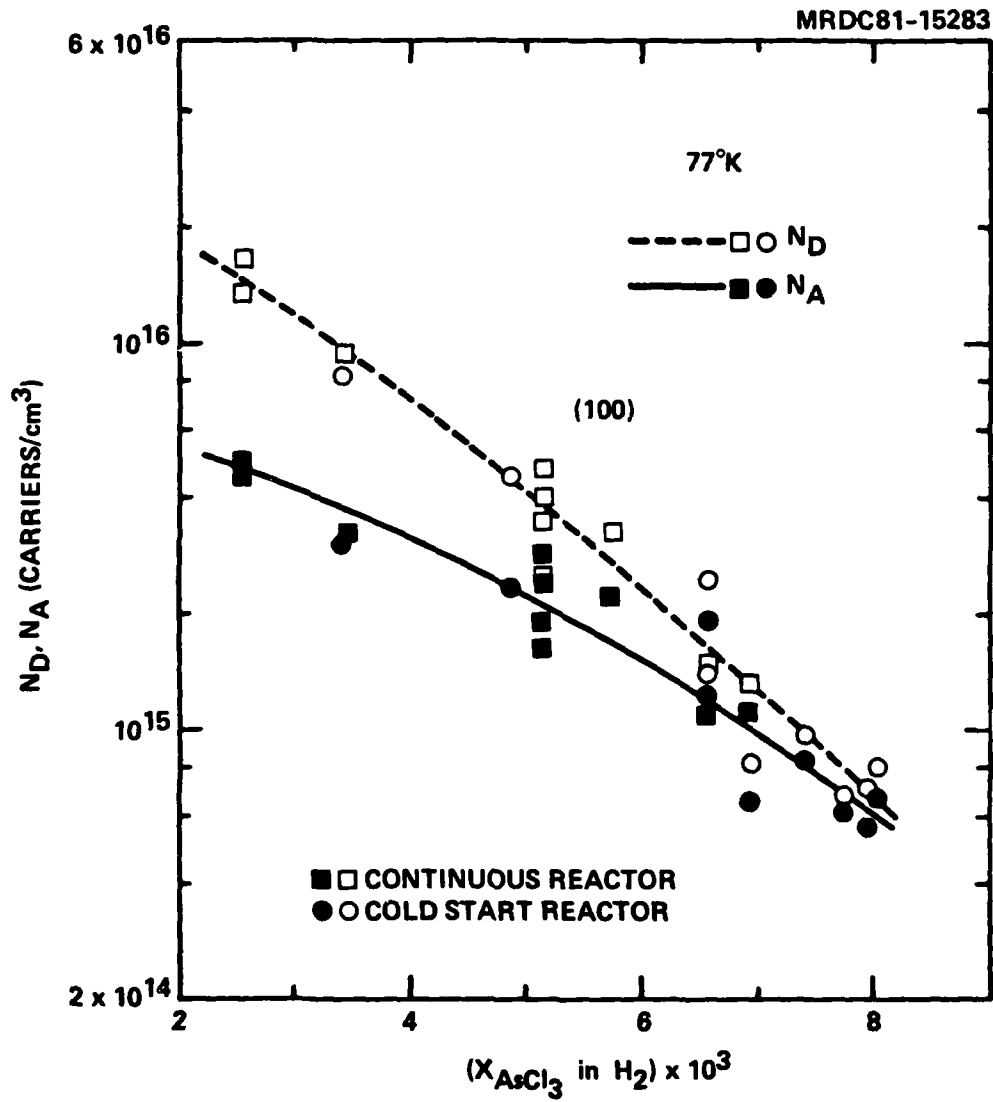


Fig. 12 VPE donor and acceptor concentration versus $AsCl_3$ mole fraction. (F33615-68-C-1136)



2.4.2 Chromium Doped Buffer Layers

Preparation Data: Doping: Cr transport from high purity Cr metal source
 AsCl_3 Mole Fraction: 1×10^{-8} to 2×10^{-3} mf
 AsCl_3 Source: Mitsubishi Lot #6425, 7-9's purity
 Gallium Source: Eagle Picher R-651K, 7-9's purity
 T_{source} : 820°C
 $T_{\text{substrate}}$: 760°C
 Flowrate: GaAs transport (330 sccm), Cr transport (50 sccm)
 Substrate: Cr doped Horizontal Bridgman E-254

Evaluation

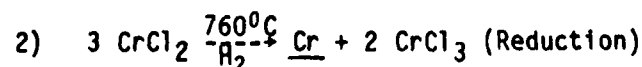
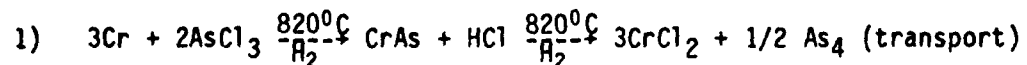
Morphology: Smooth well ordered films with slight surface texture as shown in Fig. 5.

Routine Electrical Data

Sample	Type	Approx. Net Doping	Layer Thickness	Substrates	AsCl_3 mf	Doping Input
1352	p-	$<10^{13} \text{ cm}^{-3}$	21 μm	E-254	10.6×10^{-3}	none
1353	mixed conduction	$<10^{13}$ "	7 μm	"	"	1×10^{-8} moles/l
1354	mixed cond.	$<10^{13}$ "	18 μm	"	"	5×10^{-8} moles/l
1355	mixed cond.	$<10^{13}$ "	11.3 μm	"	"	5×10^{-4} moles/l
1356	mixed	$<10^{13}$ "	11.0 μm	"	"	2×10^{-3} moles/l

Discussion

Chromium was introduced to the AsCl_3 process by vapor transport of high purity Chromium metal as follows:





Use of high purity chromium for a transport source virtually eliminates the problems associated with the defect generation that occurs with the CrO_2Cl_2 method. Due to the fact that Cr metal is transported from a CrAs source, the resulting equilibrium HCl over pressure is lower compared to that of the CrO_2Cl_2 method on a mole for mole basis. Vapor phase incorporated Chromium concentrations up to 10^{17} cm^{-3} have been produced with the Cr metal transport method without surface defect generation.⁶ Memory effects associated with remanent Cr doping are not present with the metal transport method and multilayer, in situ, growth for MESFET devices can be performed effectively as shown in Fig. 13. One of the attractive features of Cr doping is the increase in threshold voltage for space charge limited current. Cr doped buffer layers can sustain much greater voltage than the undoped buffers.⁸ High drain voltages applied to power FET devices will require tolerance to field induced ionization effects with operation at drain voltages $>10\text{V}$.

It will be advantageous to produce high resistivity buffer layers with low chromium concentrations to avoid extreme effects of compensation with the deep Cr acceptor. Figure 14 shows the SIMS profile of a Cr doped buffer layers with approximately $8 \times 10^{14} \text{ cm}^{-3}$ Cr grown upon a substrate with $4 \times 10^{16} \text{ cm}^{-3}$ Cr doping.

Analysis of Cr doped VPE Buffers by PITS shown in Fig. 15 demonstrates the domination by the deep Cr^{2+} level at $E_v + 0.89 \text{ eV}$. The data shows suppression of the native acceptor (0.83 eV) and the resolution of a deep O-related donor at $E_c - 0.67 \text{ eV}$. An additional hole trap is now prominent with Cr doping at $E_v + 0.34 \text{ eV}$. The 0.34 eV hole trap we believe is "related" to Fe doping, described more fully in Section 2.4.3. Chromium appears to be a well behaved deep level in VPE evidenced by its lack of autodoping and tendency to re-distribute at 850°C .⁶ For Cr doping $>10^{16} \text{ cm}^{-3}$ there appears to be greater thermal re-distribution effects similar to those reported in Cr doped bulk substrates.⁶ The effective compensation of shallow donor impurities is evidenced by the dramatic decrease in shallow donor activity shown in Fig. 15



CARRIER PROFILES OF SI DOPED n LAYER GROWN ON Cr DOPED BUFFER LAYER

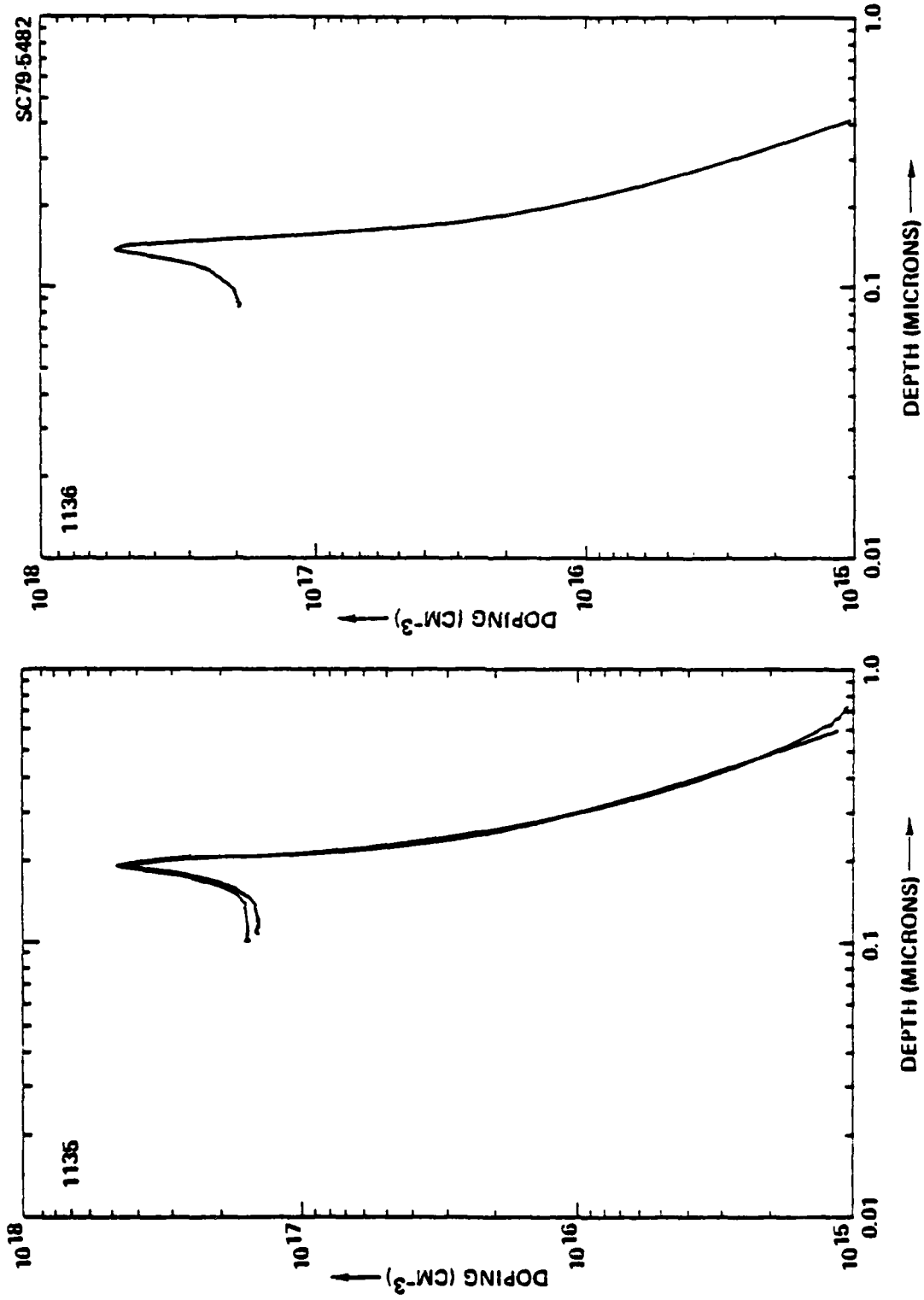


Fig. 13 Carrier profiles of active layers grown on VPE Cr doped buffers.

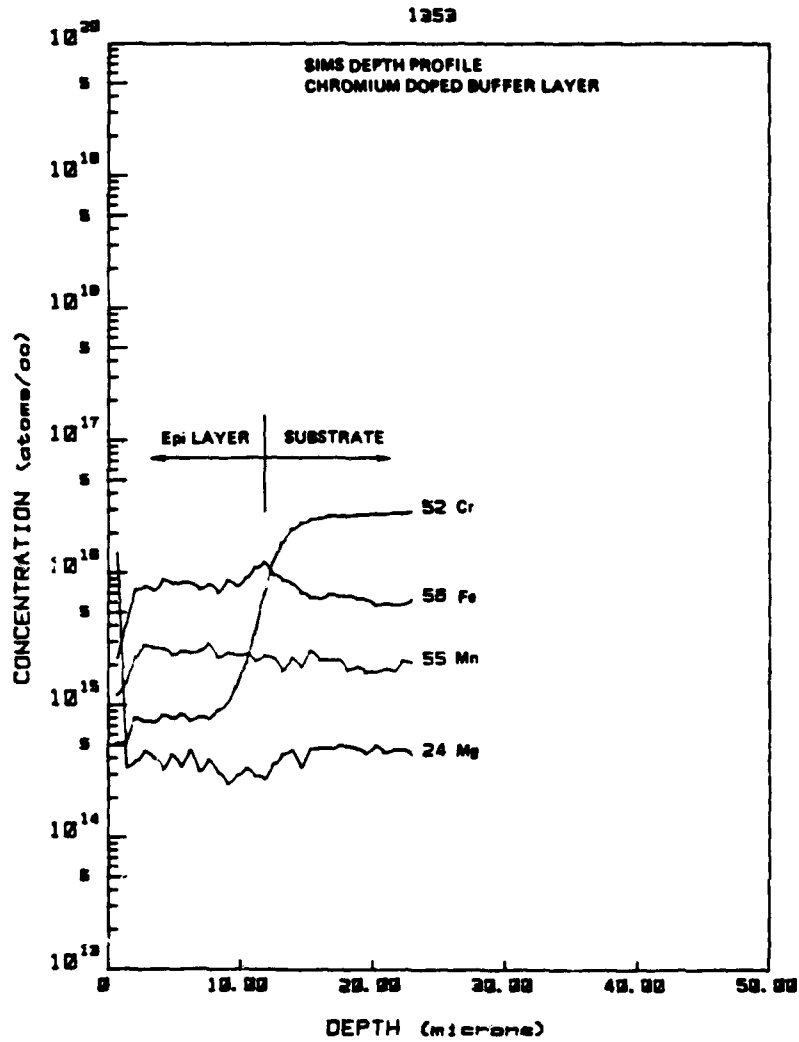


Fig. 14 SIMS depth profile, Cr doped VPE buffer layer.

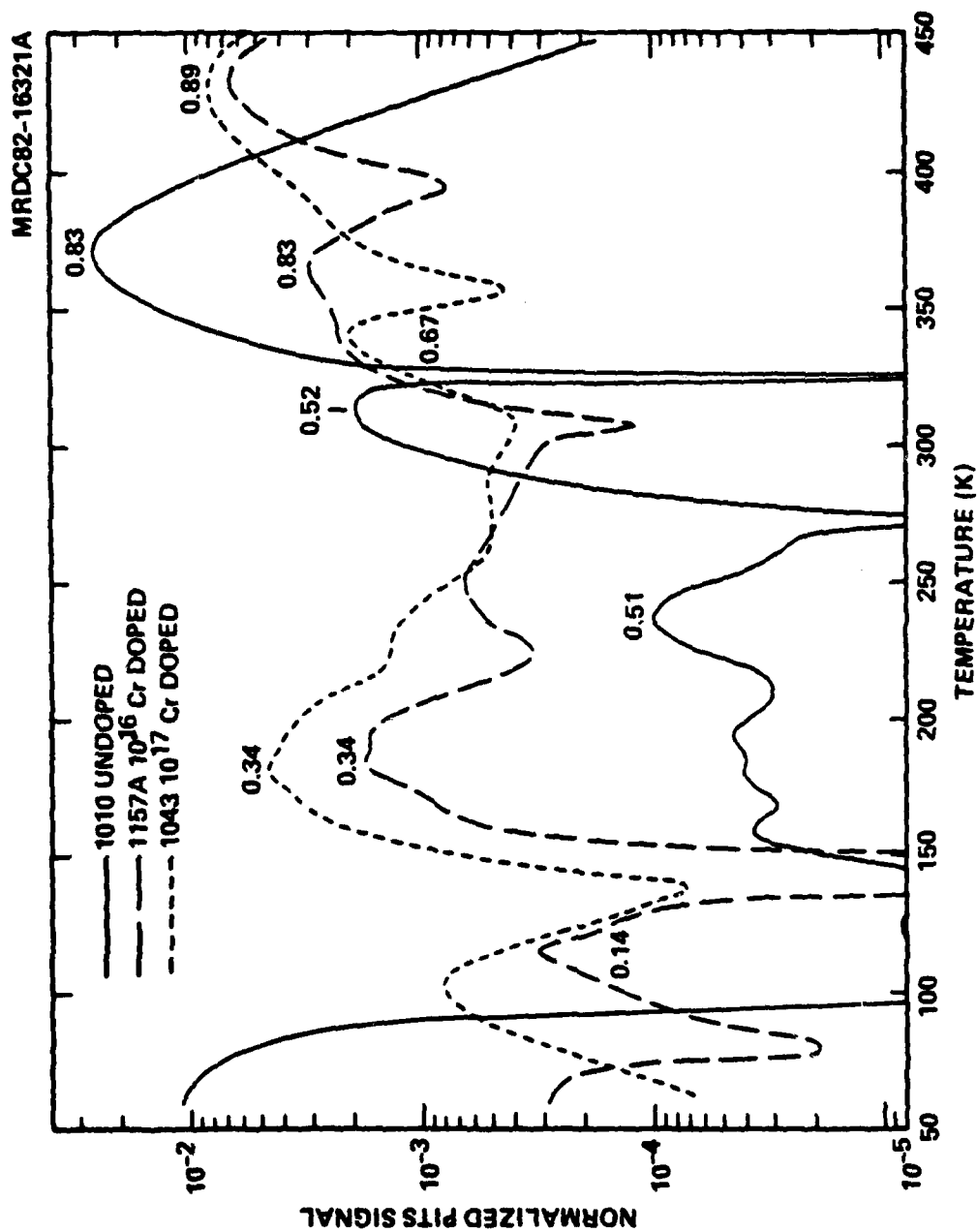


Fig. 15 Normalized photo induced transient spectroscopy, undoped and Cr doped VPE buffers.



below 60K. Using an AsCl_3 mf of 5×10^{-8} , a Cr concentration of 10^{16} cm^{-3} is achieved, which is sufficient to produce sheet resistance values $>10^9 \Omega/\square$.⁶ The thermal stability of these layers is adequate to perform ion implantation with carrier activation $>80\%$. Reproducibility of Se implants with (300 Kev, $3 \times 10^{12} \text{ cm}^{-2}$) Cr doped buffer has shown reproducibility of $\pm 8\%$, regardless of the substrate used. Since Cr^{2+} is a much deep acceptor than Fe^{2+} the Fermi level is pinned at a position, midgap, very close to the deep donor EL-2. Figure 16 shows an activation energy for Cr doped VPE at $E_v + 0.74 \text{ eV}$.

2.4.3 Iron Doped Buffer Layers

Preparation Data: Doping Fe transport from high purity Fe metal source
 AsCl_3 Mole Fraction: 1×10^{-8} to 2×10^{-2} mf
 AsCl_3 Source: Mitsubishi Lot #6425, 7-9's purity
 Gallium Source: Eagle Picher R-651 K 7-9's purity
 T_{source} : 820°C
 $T_{\text{substrate}}$: 760°C
 Flowrate: GaAs transport (330 sccm) Fe transport (50 sccm)
 Substrate: Cr doped Horizontal Bridgman E-254

Evaluation

Morphology: Smooth well order layers are observed at AsCl_3 mf $<1.1 \times 10^{-2}$ and textured surfaces above that quantity.

Routine Electrical Data

Sample	Type	Approx. Net Doping ($\rho(\Omega\text{-cm})$)	Layer Thickness	Substrate	AsCl_3 mf	Doping Input
1357	n	$<10^{13} \text{ cm}^{-3}$	20 μm	E-254	9.5×10^{-3}	none
1358	n	$\sim 10^{13} \text{ cm}^{-3}$	6 μm	"	"	1×10^{-8} moles/l
1359	p-	$<10^{13} \text{ cm}^{-3}$	17.5 μm	"	"	8×10^{-3} moles/l
1360	p-	$<10^{13} \text{ cm}^{-3}$	16.0 μm	"	"	2×10^{-2} moles/l

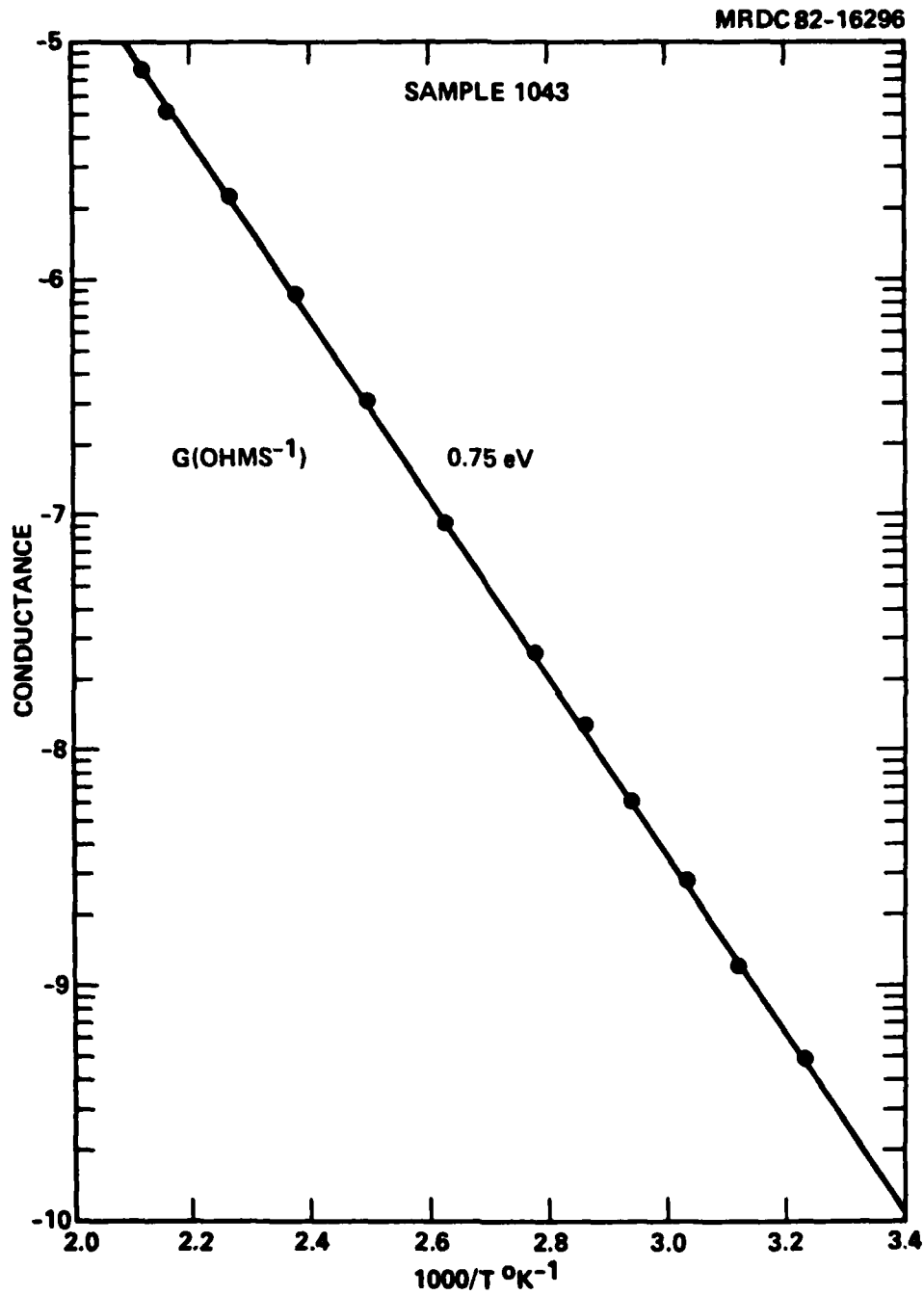
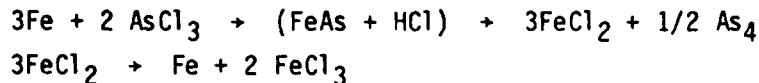


Fig. 16 Activation energy, Cr doped VPE buffer.



Discussion

High purity Fe (5-9's) was obtained from Johnson-Matthey for this work and was handled experimentally in the same manner as Cr metal sources



Vapor transport of Fe was found to be much less efficient than that for Cr and subsequently a higher AsCl_3 mf was required for vapor transport. Sample 1359 was doped to $2 \times 10^{16} \text{ cm}^{-3}$ producing a p type semi-insulating layer (Fig. 17). Iron produces a deep acceptor level at $E_v + 0.52 \text{ eV}$ as shown by PITS measurement on GaAs grown from the melt (Fig. 18). The highest resistivity obtained by Fe doping was $\sim 10^5 \Omega \text{ cm}$.⁹ Iron has demonstrated a high diffusion constant in bulk GaAs¹⁰ and is present as an undesirable impurity in Cr doped GaAs as well as undoped SI LEC crystals. Recent spark source mass spectrometry measurements have shown Fe in undoped LEC GaAs no lower than $1 \times 10^{15} \text{ cm}^{-3}$.⁵ Diffusion of Fe effects growth of the undoped VPE GaAs limiting the background concentration of Fe to $> 2 \times 10^{15} \text{ cm}^{-3}$ as measured by SIMS. At the present state of the art Fe is one of the most difficult impurities to control in GaAs and has been shown to be detrimental to power FET performance.¹¹

Iron was detected by 4K photoluminescence in all VPE layers grown in this program as well as substrates used in this study. The characteristic PL emission from Fe^{2+} is shown in Fig. 19. Using the $\Gamma_5 \rightarrow \Gamma_2$ PL emission as a measure of the electrically active Fe in the VPE layers. A relationship between Fe^{2+} emission and Fe concentration by SIMS was established (Fig. 20). The emission of Fe^{2+} is proportional to the SIMS concentration over wide range ($2-40 \times 10^{15} \text{ cm}^{-3}$) demonstrating the validity of the SIMS result. The SIMS data has a positive offset due to a residual background from stainless steel contamination in the primary ion beam. This background of Fe, and Cr is especially important for analysis at $< 2 \times 10^{15} \text{ cm}^{-3}$. A comparison was made with Spark Source Mass Spectrometry (SSMS) on substrate R7/C which by SIMS showed $2 \times 10^{15} \text{ cm}^{-3}$, a result of $1 \times 10^{15} \text{ cm}^{-3}$ by SSMS indicated that our results above $2 \times 10^{15} \text{ cm}^{-3}$ should have reasonable accuracy for Fe.¹²

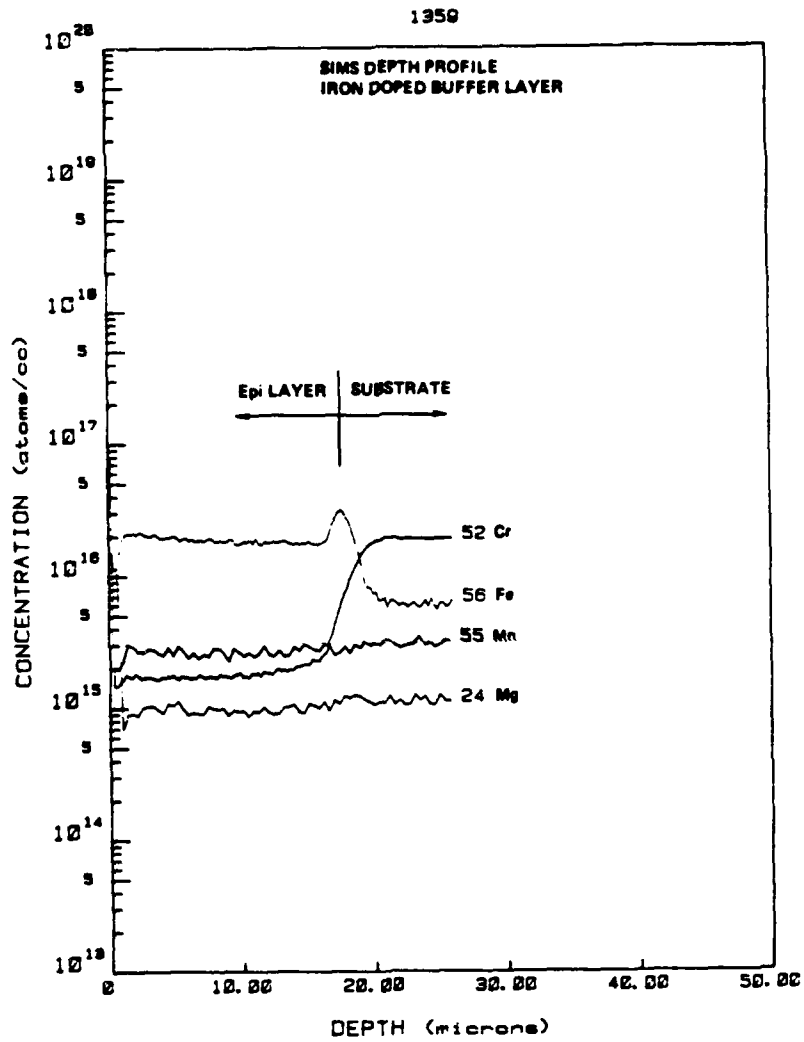


Fig. 17 SIMS depth profile, Fe doped VPE buffer layer.

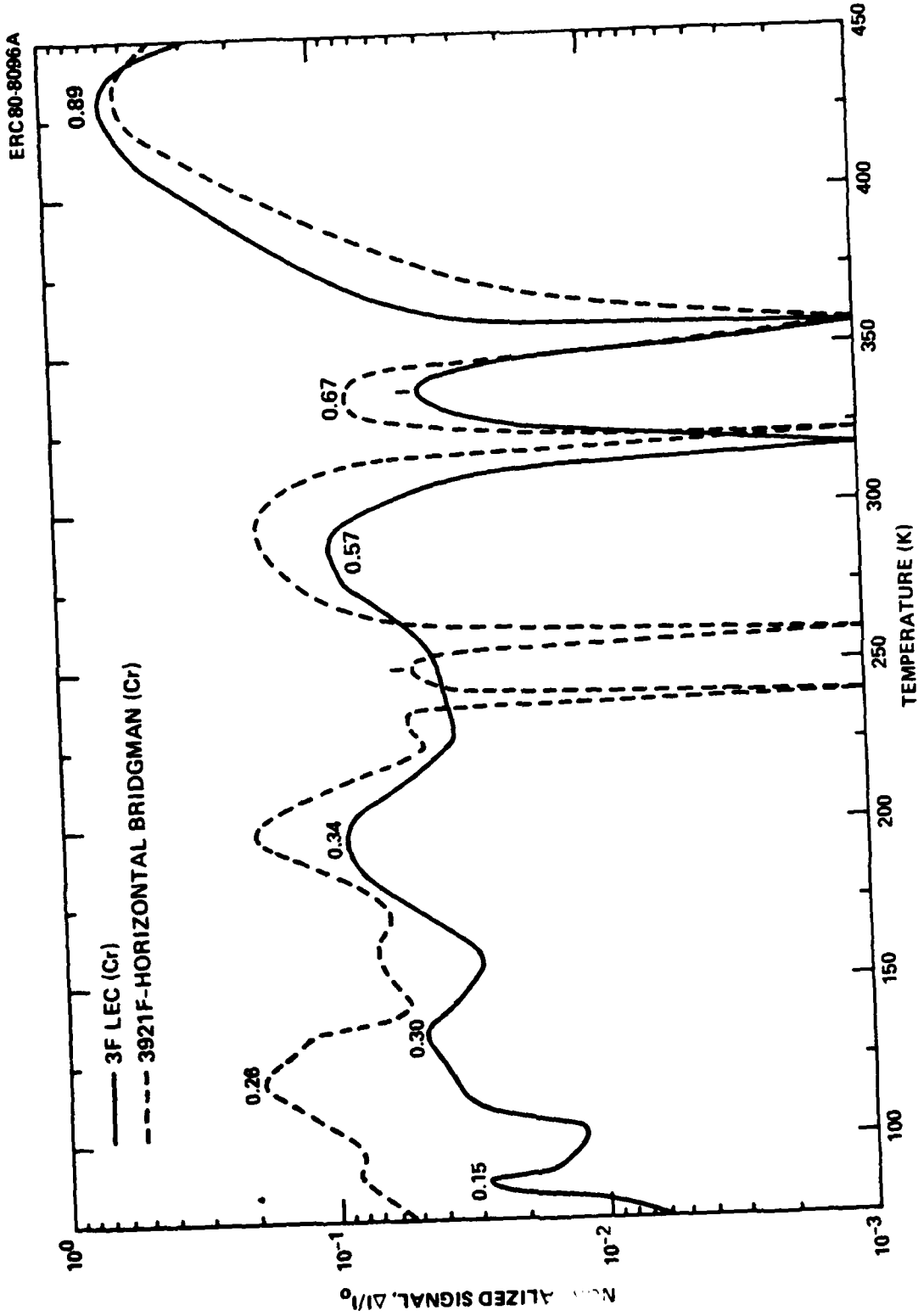


Fig. 18 Normalized photo induced transient spectroscopy, Cr doped bulk GaAs.

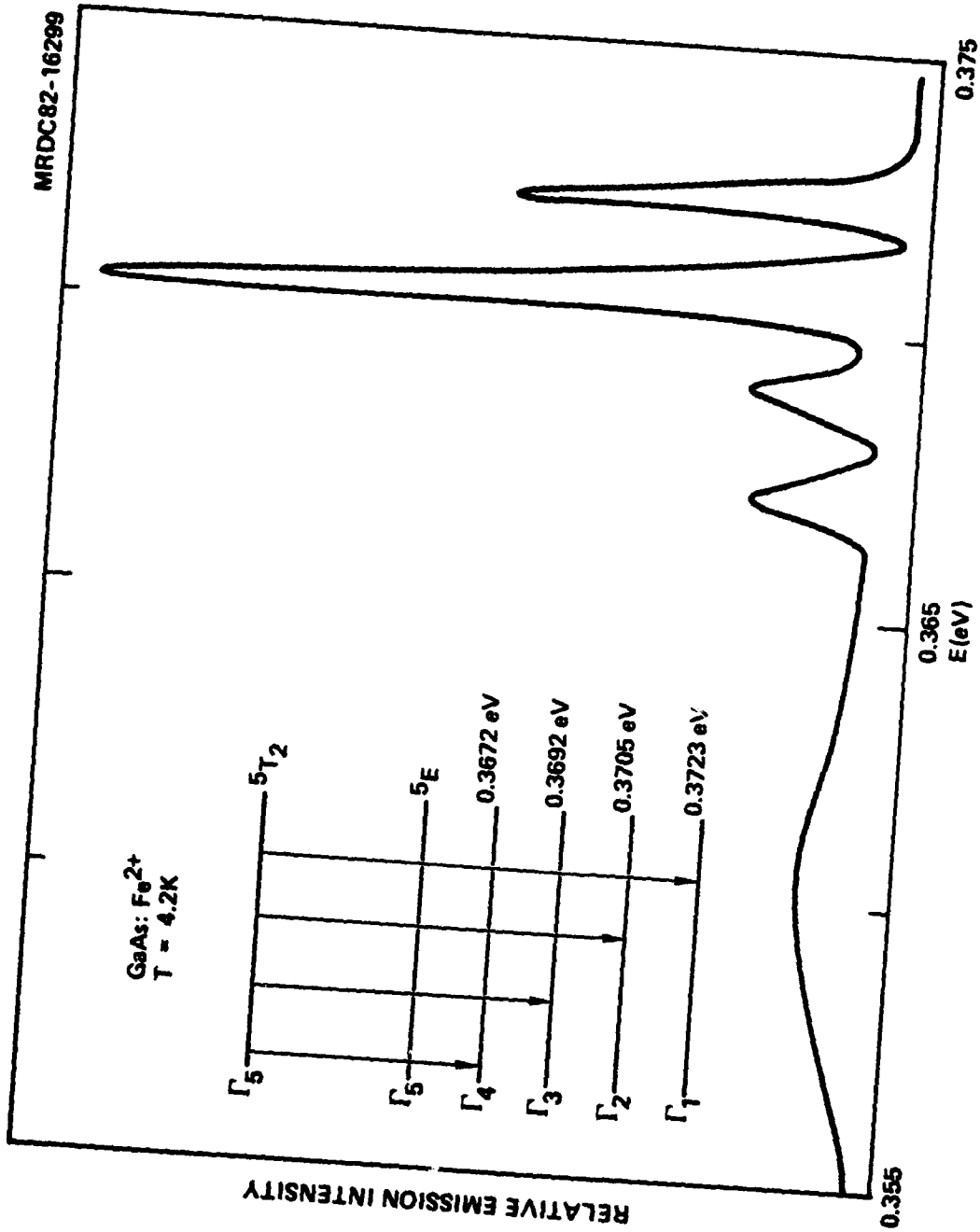


Fig. 19 4K photoluminescence spectra, Fe in GaAs.

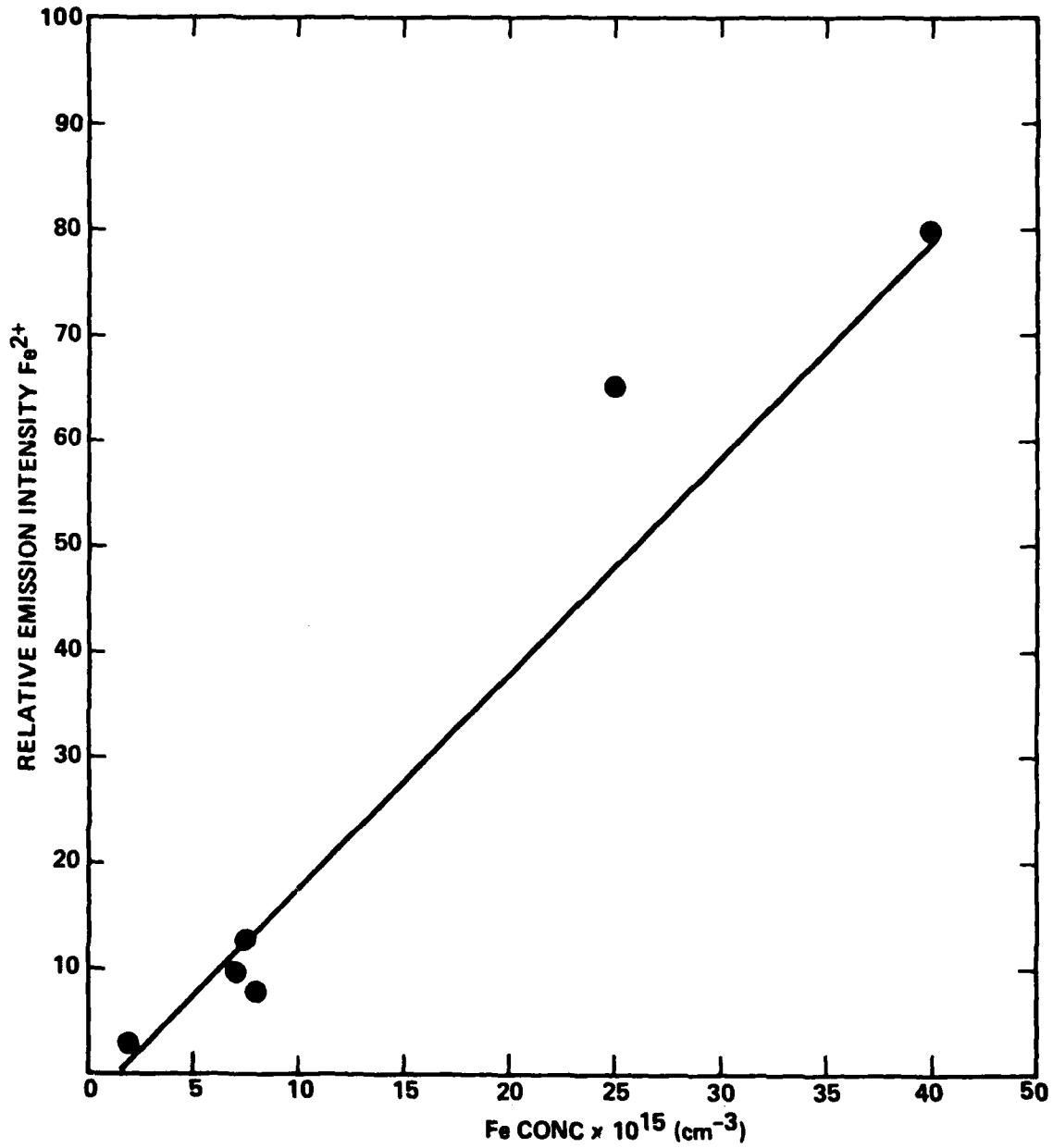


Fig. 20 4K photoluminescence, Fe^{2+} versus SIMS concentration, VPE GaAs.



Photo Induced Transient Spectroscopy (PITS) measurements shown in Fig. 21 on Fe doped sample 1359 revealed enhanced trap emission for both the $E_v + 0.52$ eV and $E_v + 0.34$ eV levels. Emission from a $E_v + 0.40$ eV and 0.18 eV level were also observed and will be described in the PITS measurement summary, Table 1. An activation energy measurement shown in Fig. 22 for Fe taken from conductance vs temperature data reveals the dominant $E_v + 0.52$ eV hole trap which correlates well with previous workers.^{13,14,15} The $E_v + 0.34$ eV hole trap has been observed in many samples coincident with the dominant $E_v + 0.52$ eV Fe^{2+} center. It is postulated that the 0.34 eV hole trap is an Fe-related complex.

2.4.4 Oxygen Doped Buffer Layers

Preparation Data: Dopant: $^{18}O_2$, enriched 96-98%, Monsanto
Research Corp.

Arsenic Trichloride: Mole Fraction 9.5×10^{-3}

Arsenic Trichloride Source: Mitsubishi lot #6425,
7-9's purity

Gallium Source: Eagle Picher R-651K,
7-9's purity

T_{source} : $820^\circ C$

$T_{substrate}$: $760^\circ C$

Flowrate: GaAs transport (330 sccm), $^{18}O_2/H_2$
(10 sccm)

Substrate: Undoped LEC, 3-28

Evaluation: Morphology: Smooth well ordered layers with slight texture as shown in Fig. 23. O_2 doping concentrations up to 1430 ppm had no apparent effects upon surface morphology or defect generation.

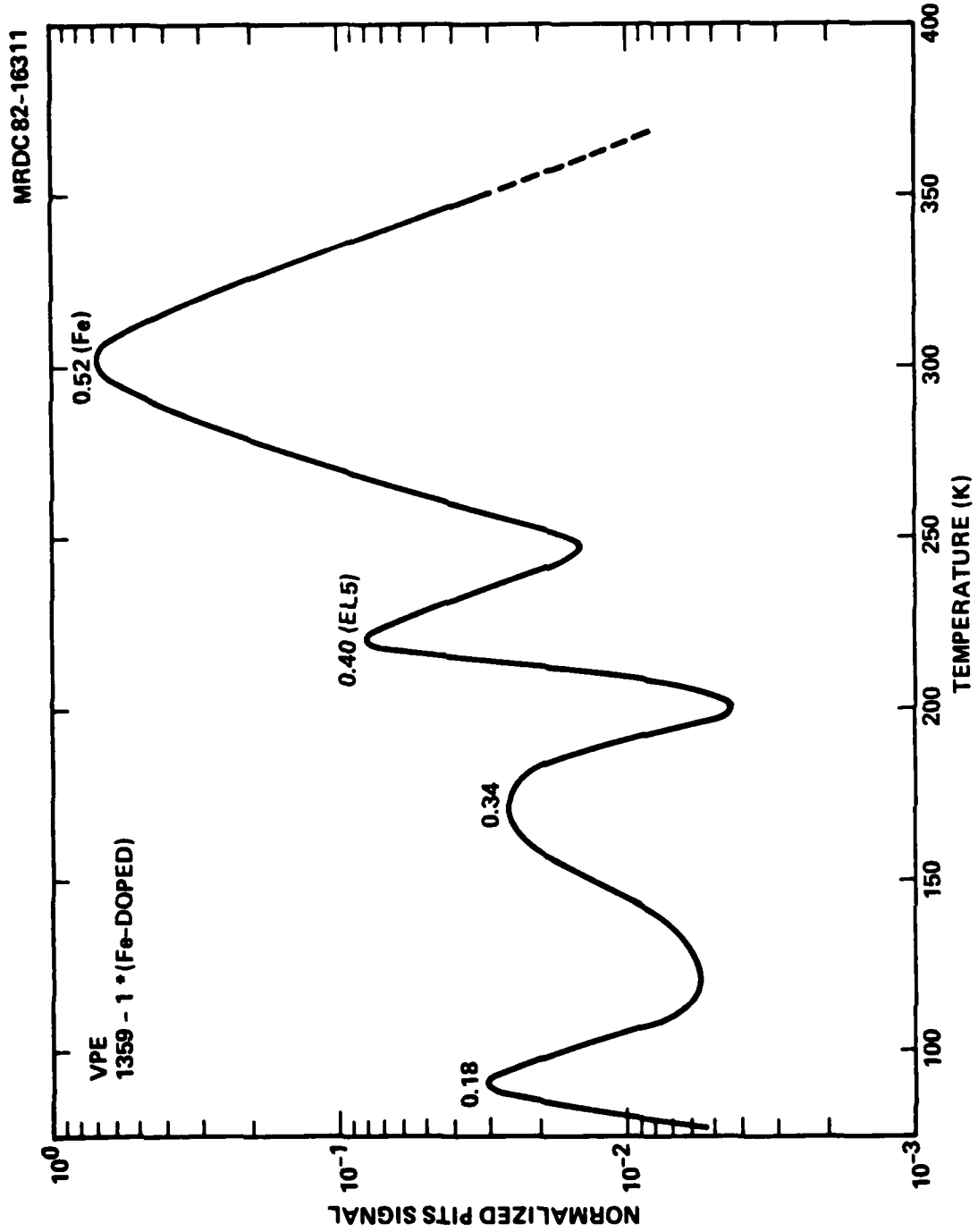


Fig. 21 Normalized PITS spectrum, Fe doped buffer.

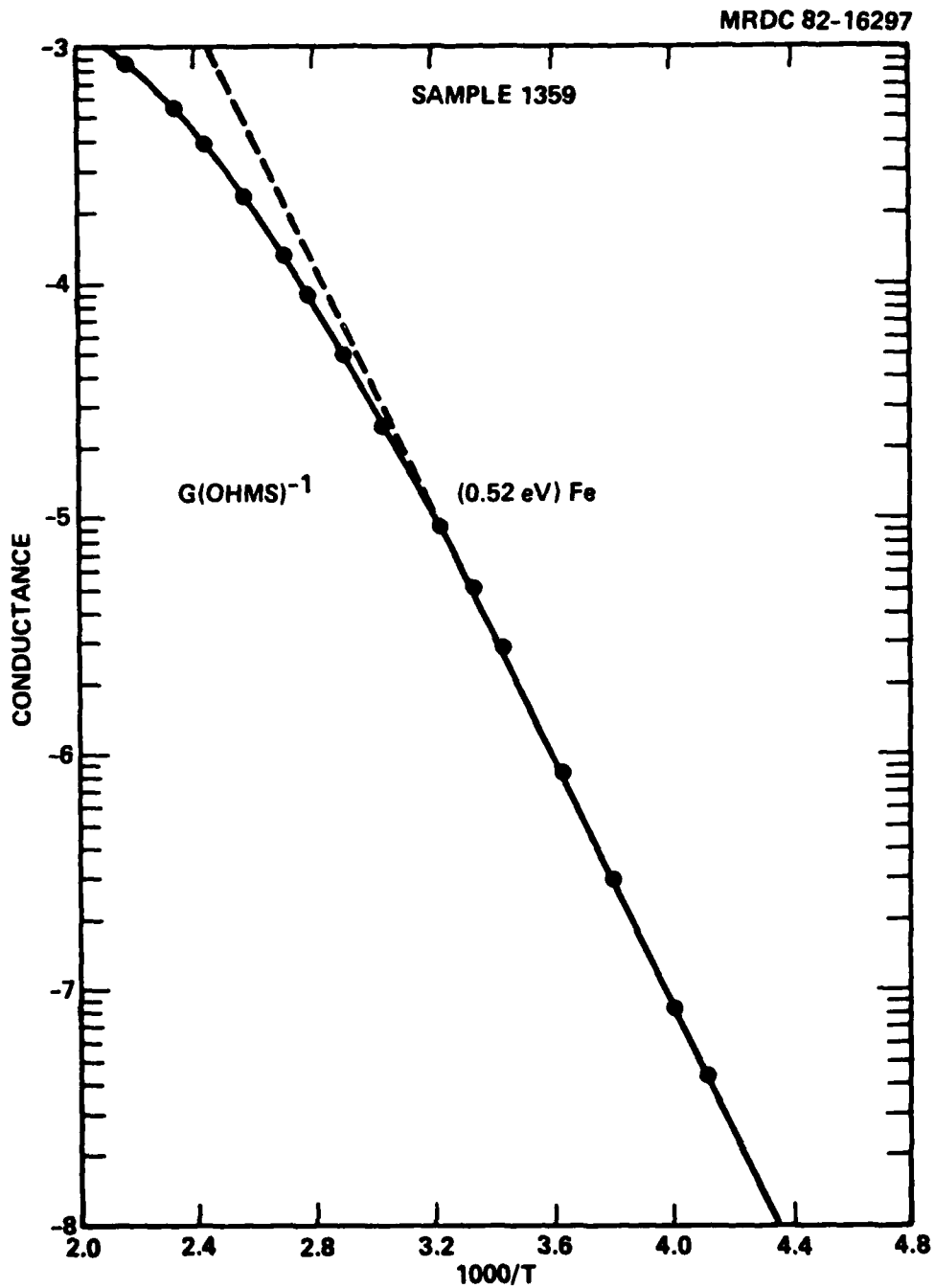
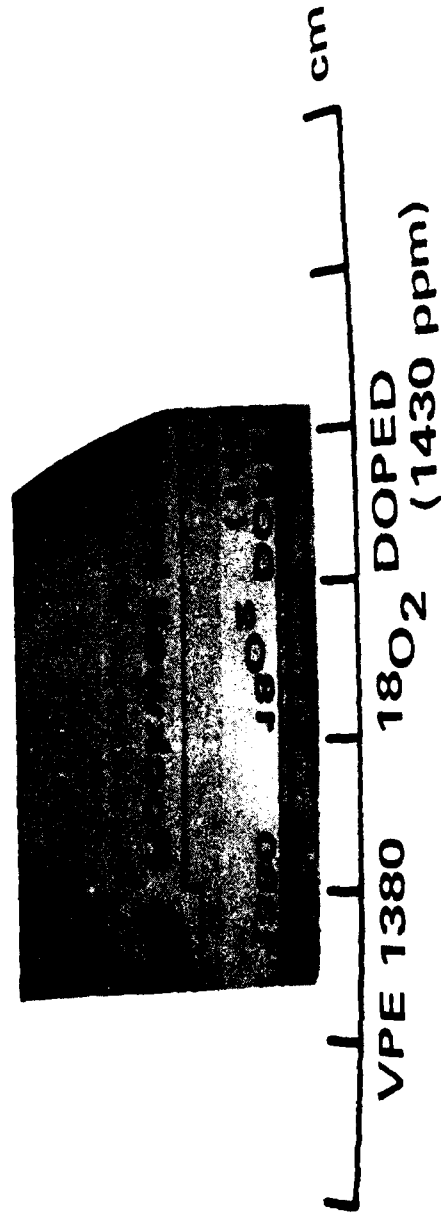


Fig. 22 Activation energy, Fe doped buffer.

MRDC82-17589



 **Rockwell International**



Rockwell International

MRDC41086.2ARF

Fig. 23 Surface morphology, oxygen doped VPE buffer layer.

Routine Electrical Data

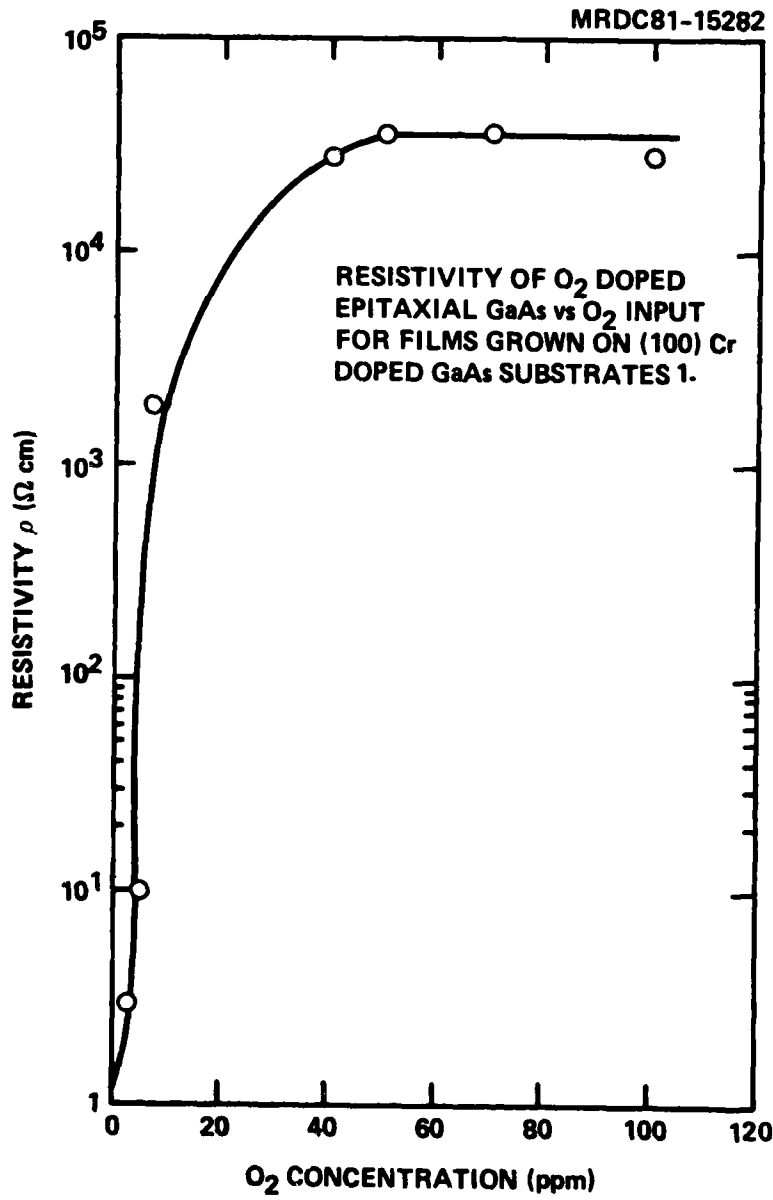
Sample	Type	Approx. Net Doping (cm ⁻³)	Layer Thickness	Substrate	AsCl ₃	C ¹⁸ O ₂ (ppm)
1381	p-	<<10 ¹³ cm ⁻³	40 μm	Undoped LEC C3-28	10.6×10 ³	none
1381	n	~10 ¹⁴ cm ⁻³	24 μm	" "	9.5×10 ³	none
1375	p-	<10 ¹³ cm ⁻³	26 μm	" "	" "	129 ppm
1377	p-	<10 ¹³ cm ⁻³	18 μm	" "	" "	247 ppm
1380	p-	<10 ¹³ cm ⁻³	40 μm	" "	" "	1430 ppm

Discussion

Oxygen has been described as a deep donor impurity in GaAs¹⁶⁻²⁰ and has been the source of conflicting claims since 1960. Effects of O₂ doping in GaAs have been reported for bulk crystal growth^{17,19} VPE^{20,21} and MBE growth.²² The role of oxygen in reducing the Si content of bulk crystal growth has been well confirmed.

Carrier removal effects in O₂ doped VPE GaAs are coincident with the growth of a deep donor at E_v - 0.67 eV. SIMS analysis indicates no change in the Si concentration between O₂ doped or undoped VPE GaAs suggesting the carrier removal by O₂ occurs with a Si on a Ga site. Epitaxial layer resistivity produced by O₂ doping compares well with earlier work shown in Fig. 24. Conductivity type changes from n → p between 5-10 ppm O₂. Maximum resistivity obtained with O₂ doping is always in the range of 10⁴ - 10⁵ Ω cm for thick layers with mobilities no greater than ~300 cm²/V-s at 300K as expected for Fe doping.

In order to define the role of O₂ in GaAs a source of ¹⁸O₂ was used to dope VPE layers 1375, 1377 and 1380. SIMS was used to check the chemical content of these layers independent of trace O₂ contaminants in the epitaxial reactor, SIMS spectrometer or sample surface. SIMS sensitivity for ¹⁸O₂ has been quoted at ~ 8 × 10¹³ cm⁻³ and free from most interferences.²³



1. WITH PERMISSION FROM FAIRCHILD CAMERA & INSTRUMENT CORP.

Fig. 24 Resistivity of O₂ doped VPE buffer versus O₂ concentration.



Concentrations of O_2 up to 1430 ppm were used in the layers in order to provide a suitable sample for analysis. No detectable $^{18}O_2$ was observed from the SIMS analysis as performed (Fig. 25, 26). The $^{18}O_2$ tracer method has been used successfully with bulk Si to determine O_2 content down to the 10^{15} cm^{-3} level by SIMS.²³ Verification of our $^{18}O_2$ doping source was made by mass spectrometry (Fig. 27) and was found to be correct as supplied by Matheson Research Corp. Electrical measurements on the " $^{18}O_2$ doped" layers showed lower resistivity in the 10^3 - $10^4 \Omega \text{ cm}$ range, all p type. The layers were grown with an $AsCl_3$ mf of 9.5×10^{-3} which without O_2 produced n type - 10^{14} cm^{-3} doping. All experiments were performed with undoped SI LEC substrates to minimize the substrate contributions to epitaxial layer doping. Similar results of low O_2 solubility have been reported by other workers indicating the difficulty in determining its value in GaAs.²⁴

Indirect evidence for O_2 doping has been obtained concerning the behavior of oxygen in GaAs by photo induced transient spectroscopy shown in Fig. 28. A prominent trap emission peak at $E_c - 0.67 \text{ eV}$ is shown occurring at 320K. The O-related peak has been observed in most all semi-insulating GaAs measured by PITS and was first described by Oliver et al⁷ as being O-related in undoped LEC GaAs grown with water doped B_2O_3 . A very prominent Fe^{2+} center ($E_v + 0.52 \text{ eV}$) was observed in the shoulder of the O-related peak. The remaining centers at 80K, 260K and 400-450K are less significant and are described in the summary of PITS measurement, Table 1. The most important parameter significant for O_2 -doped GaAs is the activation energy, of the dark conductivity as shown in Fig. 29, determined by the slope of an Arrhenius curve of conductance vs temperature. In this case the deep Fe^{2+} acceptor at $E_v + 0.52 \text{ eV}$ was shown to be the dominant center controlling type and resistivity. Carrier removal of Si with O_2 checks very well with the low temperature end of the PITS Fig. 28, where the other PITS data (Fig. 15) show strong residual signals below 150K.

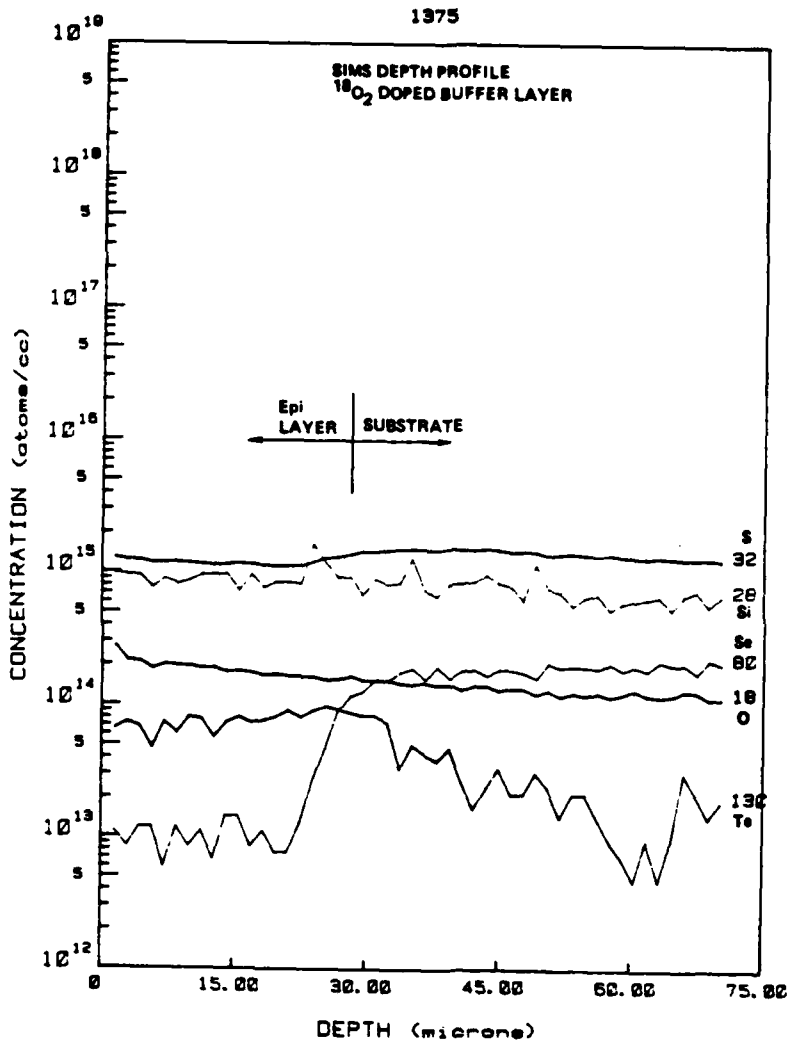


Fig. 25 SIMS depth profile, $^{18}\text{O}_2$ doped VPE buffer 1375.

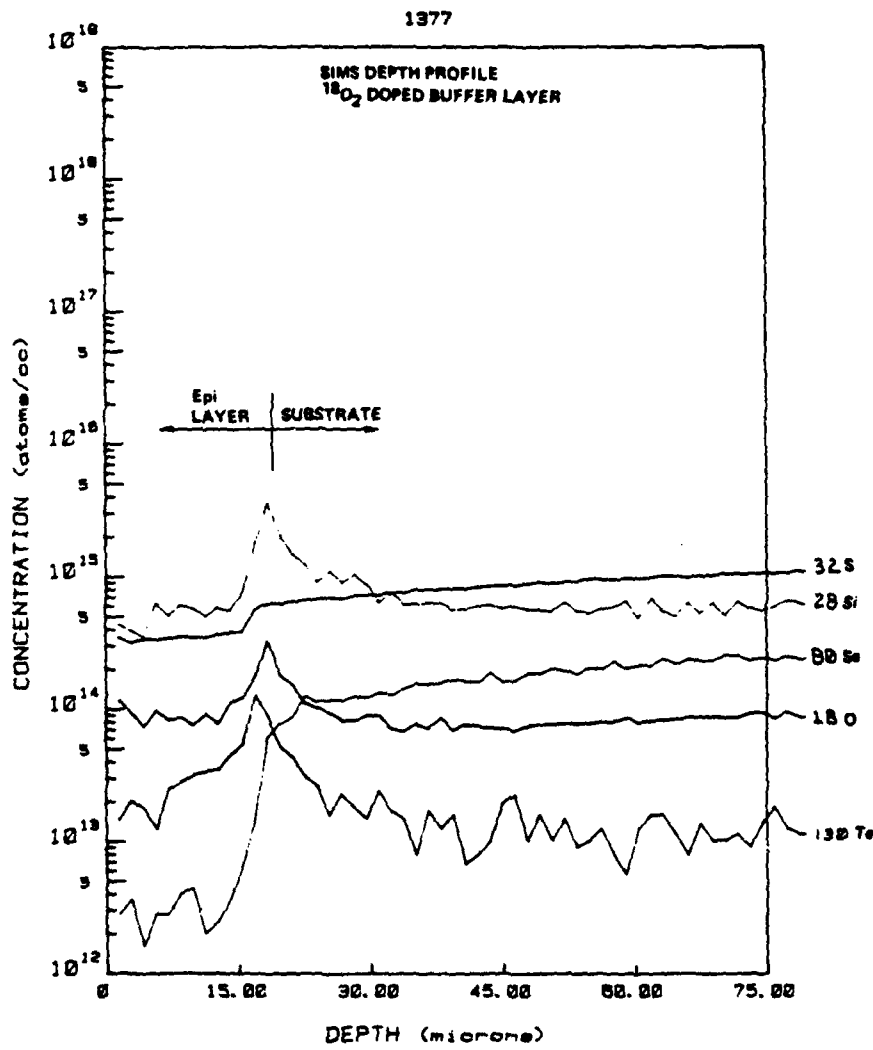


Fig. 26 SIMS depth profile, $^{18}\text{O}_2$ doped VPE buffer 1377.

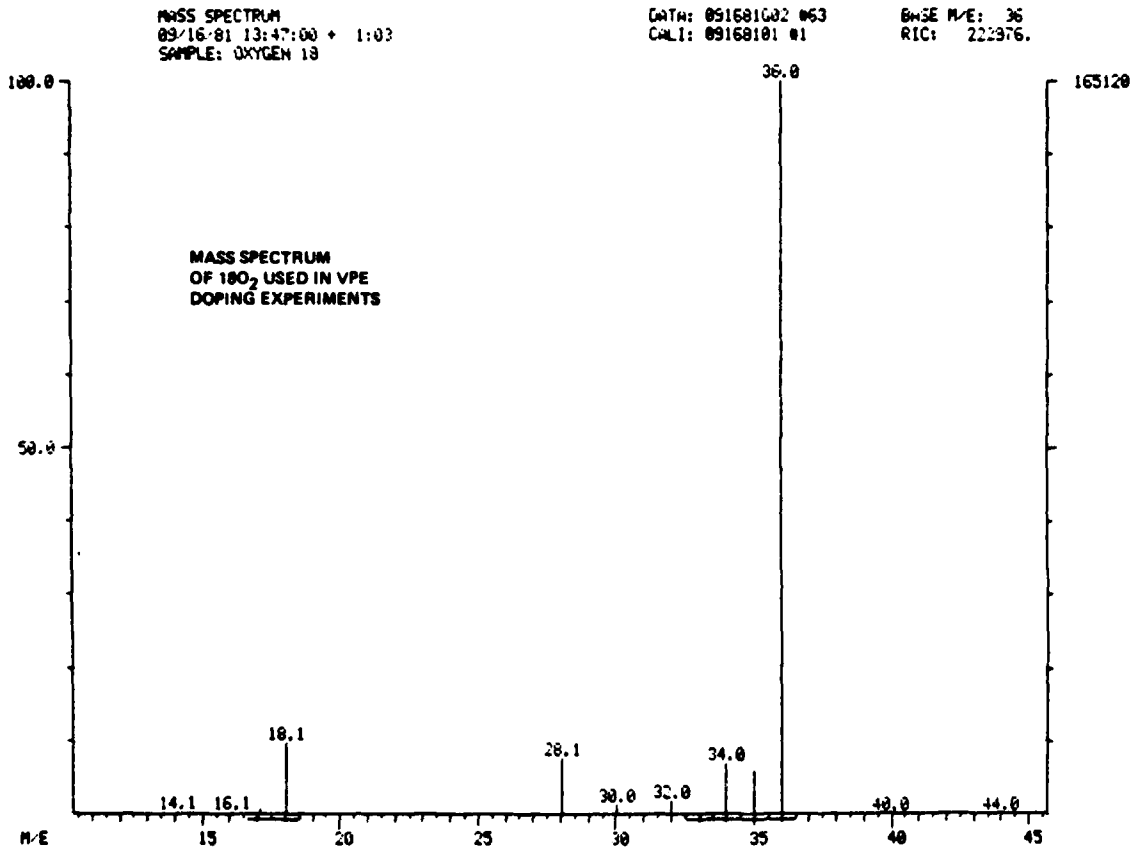


Fig. 27 Verification of $^{18}\text{O}_2$ dopant by mass spectrometry.

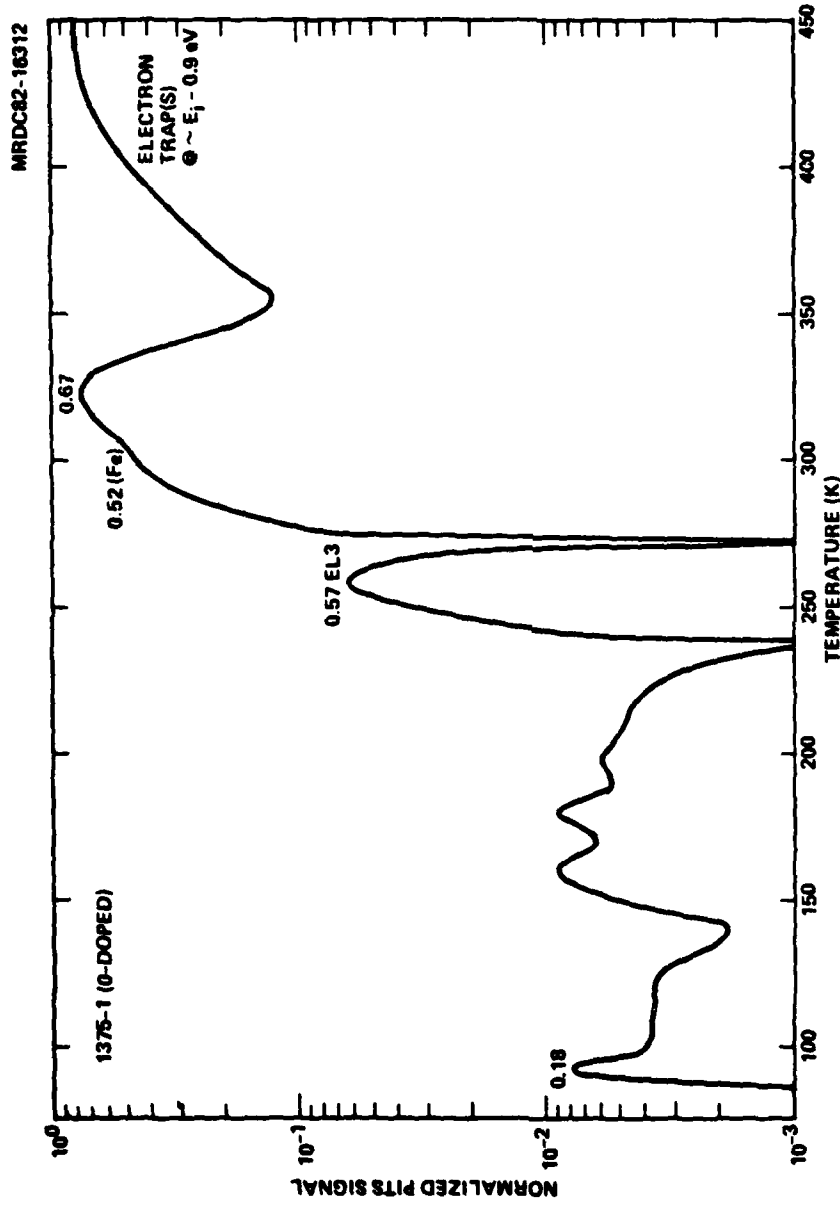


Fig. 28 Normalized PITS spectrum, $^{18}O_2$ doped buffer.

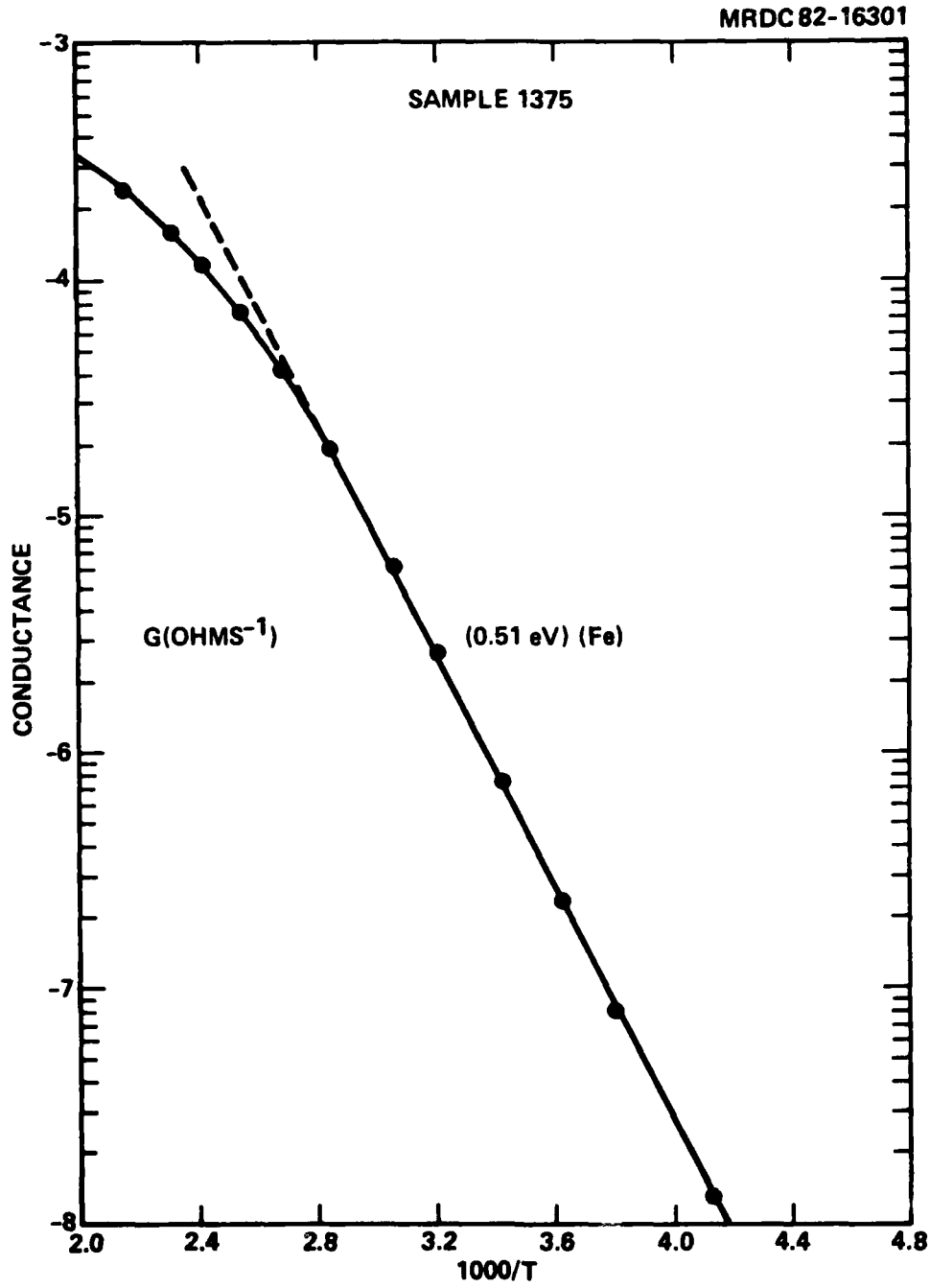


Fig. 29 Activation energy, $^{18}\text{O}_2$ doped buffer.



2.4.5 Summary of Progress to Date

Overall progress in the initial phase of the epitaxial buffer layer technology program has revealed several important facts concerning growth and control of high resistivity undoped and compensated buffer layers.

The use of lightly Chromium doped and undoped LEC substrates has allowed the analysis of very subtle deep level contamination of the VPE buffer layer growth. New characterization techniques such as improved SIMS, 4K Photoluminescence and Photo Induced Transient Spectroscopy have allowed valuable cross correlation of experimental data. The multitude of new trapping center data from both undoped and intentionally compensated buffer layers has required careful assessment of the Fermi level position and activation energy to determine the dominant center in these materials.

Undoped Buffer Layers

Considerable emphasis was given to the so called undoped buffer layer beginning in 1968. Following the discovery of Cr out-diffusion in GaAs and the use of heavily Cr doped, semi-insulating, substrates it has become apparent to several workers that the high resistivity buffer layers are unintentionally Cr compensated. Efforts in this program to realize "intrinsic" buffer layers by VPE growth on lightly Cr doped or undoped LEC substrates have led to layers with lower resistivity and the detection of anomalous Fe diffusion during epitaxy due to the fact that all available GaAs substrate materials are contaminated with Fe in the range of $1-20 \times 10^{15} \text{ cm}^{-3}$. This result has been independently substantiated by Y_u and co-workers using 4K photoluminescence, SIMS and SSMS measurements.⁵

Electrical measurements of undoped buffers grown on the undoped LEC substrates have led to p-type layers due to Fe contamination in the substrate. Hall measurements performed on VPE layers indicate p-type behavior and a low resistivity in the $10^4 \text{ } \Omega\text{cm}$ range.²⁷ The Fe^{2+} center at $\text{Ev}+0.52 \text{ eV}$ has been detected by PITS and is established as the dominant center by dark conductivity Fermi level measurements. The SIMS profile suggests a vacancy enhanced mechanism permitting Fe to redistribute during epitaxial growth.



Table 1
Traps Observed in LEC GaAs From PITS

E_T (eV) ⁽¹⁾	σ (cm ²) ⁽²⁾	Identity ⁽³⁾	Comments
→ 0.15	8E-14(n)	-	
→ 0.18	8E-13(n?)	-	
0.14	1E-16(n)	EL11	
0.26	2E-12(n?)	-	
0.28	2E-12(n?)	-	
0.30	4E-14(p)	HL6	
→ 0.34	5E-14(n)	EL6	
→ 0.34	2E-13 (p)	HL-7?	
0.26	1E-16(n)	-	Si-O acceptor complex 0.22eV from dark conductivity
→ 0.40	5E-14 (n)	EL5	
→ 0.51	9E-13(n)	EL4	
→ 0.57	6E-13(n)	EL3	
→ 0.52	1E-15 (p)	HL8	Fe. Prominent with Cr-doping
→ 0.65 - 0.67	8E-14(n)	-	[O]-related. Also from dark cond.
→ 0.83	2E-13(p)	HL10	
→ 0.89	3E-14(p)	HL1	Cr acceptor
→ (0.74)	8E-14(n)	EL2	(From dark, DLTS conductivity)

- (1) Energy referred to 0°K bandgap, including energy (if any) associated with the cross-section.
- (2) Uncorrected for temperature dependence of band-gap.
- (3) From G. M. Martin, A. Mitonneau and A. Mircea, Electronics Letter 13, No. 7, p. 191, and No. 22, p. 666 (1977).
- Observed in VPE GaAs Buffer Layers



Successful growth of n-type undoped semi-insulating buffer layers has been accomplished by the use of substrates with $<2 \times 10^{15} \text{cm}^{-3}$ Fe and higher shallow donor concentrations.

Chromium Doped Buffer Layers

Chromium doping has been responsible for stable, reproducible buffer layers grown with CrO_2Cl_2 or by direct transport of high purity Cr metal.⁶ The outdiffusion of Cr from buffer layers with $<10^{16} \text{cm}^{-3}$ Cr, at VPE temperature is minimal. Re-distribution of Cr from layers doped to $\sim 10^{16} \text{cm}^{-3}$ is minimal and has permitted reproducible Se ion implantation ($\pm 8\%$) to be attained.⁶ Implanted layers with peak doping as low as 10^{16}cm^{-3} and carrier activation $>90\%$ have been observed. Whenever Cr is present in concentration greater than the residual Fe the equilibrium fermi level is pinned at $E_c - 0.74 \text{ eV}$ and resistivity is $>10^6 \Omega\text{cm}$. Multilayer power FET's produced with Cr doped buffers (H. Fukui et al²⁹) have shown excellent device performance and reliability under high temperature bias stress and RF conditions for period in excess of 3000 hours. Chromium doping in our work has produced semi-insulating epitaxial layers with excellent thermal stability and reproducible carrier activation.

Iron Doped Buffer Layers

Experience with un-intentional and deliberate Fe doping from high purity Fe sources (5-9's) has produced epitaxial layer resistivity no greater than $5 \times 10^4 \Omega\text{cm}$. Fe does not occupy a level as deep as Chromium and thus all traps above Fe^{2+} will be empty and active trapping centers offering greater activity in active device operation compared to compensation by Cr^{2+} . The $E_v + 0.34$ hole trap formerly associated with Cr doping has been related to Fe thru selective doping with high purity Fe metal. The 0.34 eV Fe related hole trap is most likely a complex and deserves further study.

Intentional Fe doping has been a useful technique to substantiate the identity of Fe as a substrate contaminant by 4K photoluminescence, SIMS and PITS measurements.



Oxygen Doped Buffer Layers

Oxygen has long been labeled as a deep, compensating donor impurity. In this work we have substantiated the following:

- 1) O_2 doping induces a $E_v-0.67$ eV center
- 2) O_2 thru carrier removal of Si allows residual Fe^{2+} to dominate in O_2 doped buffers producing p-conductivity.
- 3) Assessment of O_2 solubility in GaAs by $^{18}O_2$ doping was not successful by SIMS analysis. Further work will be required to make an accurate assessment.

The " O_2 related" center at $E_c-0.67$ eV is the same level measured in undoped LEC GaAs grown from wet B_2O_3 .⁷ 4K photoluminescence was not observed from these heavily doped VPE layers (>100 ppm O_2) due most likely to quenched luminescence effects. Recently several workers have observed the same deep level related to O_2 from bulk GaAs^{25,26} and from O_2 ion implanted samples²⁷ using DLTS measurements. Oxygen we believe is a detrimental impurity that can effect carrier reduction and induce compensation in GaAs. By careful control of system integrity using Helium-vacuum leak detection O_2 contamination can be minimized.

2.5 Recommendations

An energy level diagram shown in Fig. 30 represents an overview of our present status in impurity modeling for VPE GaAs buffer layer growth. At this point it is important to clarify several results that have critical bearing on future work.

A classification of impurities in GaAs is shown in Table 2 along with present methods of controlling sources of doping.

In the growth of undoped semi-insulating n-type buffer layers it is extremely important to eliminate Fe as we have shown in growth of buffers with minimum donor concentrations. The Ge, Zn, Mg, Mn and C acceptor impurities



MRDC81-15366B

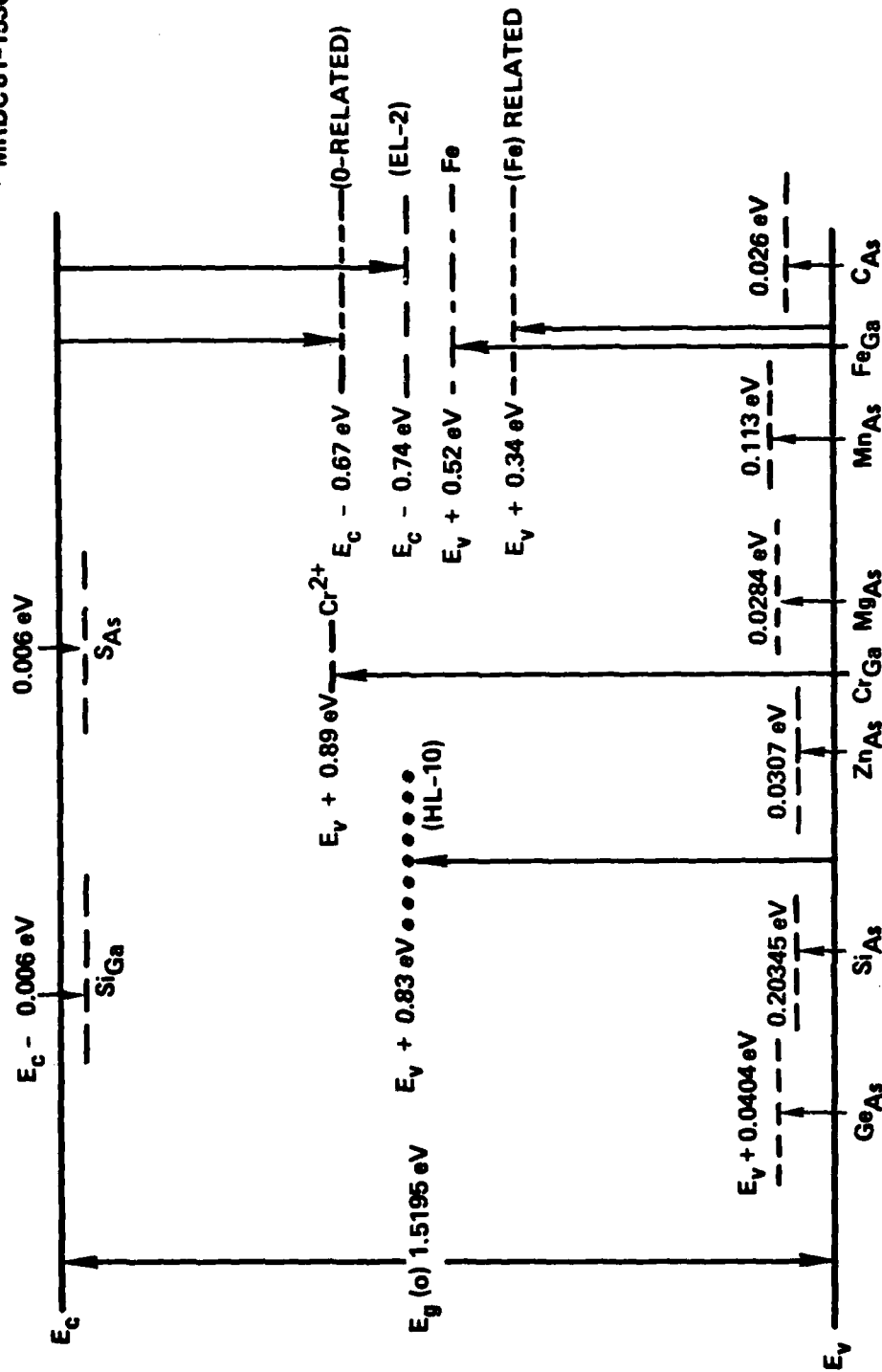


Fig. 30 Energy level diagram, VPE buffer summary.



were minimized by using undoped LEC substrates. Both Cr and S are also very low in undoped LEC GaAs. Residual Fe is a major problem in all bulk substrates and individual assessment by 4K photoluminescence or atomic absorption should be made prior to purchase. Residual O_2 from reactor tube dissociation (SiO_2) is estimated in the 0.1 - 0.8 ppm range by the reaction thermodynamics of SiO_2 with H_2 and HCl .²⁸

Table 2
Impurity Summary

Impurity Classification	Source of Doping	Means of Control
<u>Shallow Donors</u>		
Si	Fused silica reactor tube	Use minimum effective reactor temperatures, high AsCl ₃ mf
S	AsCl ₃ source	Quality control by AsCl ₃ vendor, H ₂ purge before use.
<u>Shallow Acceptors</u>		
Ge Zn Mg Mn C	GaAs substrate	Use higher purity undoped LEC substrates
<u>Deep Levels</u>		
Cr	GaAs substrate	Use higher purity undoped LEC substrate
Fe	GaAs substrate	Obtain higher purity undoped LEC substrates
O ₂	Dissociation of fused SiO ₂ reactor tube/unintentional leaks in reactor system	



Suppression of native deep levels such as HL-10 and EL-2 are possible yet not well understood at present. A re-evaluation of the effects of stoichiometry on the above levels with respect to the AsCl_3 mf is required in light of the recent improvement in characterization methods for deep levels.

A study of impurity complexes is appropriate for the (0) related center ($E_c - 0.67$ eV) and the (Fe) related center ($E_v - 0.34$ eV) for future work on VPE buffers. The question of Cr doping will need to be answered on a device performance basis. At present it is apparent that Cr doped GaAs possesses greater high field properties than the undoped semi-insulating GaAs which are important for discrete devices sustaining high electric fields or high density integrated circuits in GaAs.



3.0 REFERENCES

1. W. F. Finch and E. W. Mehal, "Preparation of $\text{GaAs}_x\text{P}_{1-x}$ by Vapor Phase Reaction," J. Electrochem Soc., 111, 814 (1964).
2. L. Hollan, "Vapor Phase Epitaxial Growth of GaAs for Multiple Applications," Gallium Arsenide and Related Compounds 1974, Inst. Phys. Conf. Soc. 24, p. 22, (1975).
3. R. D. Fairman and R. Solomon, "Submicron Epitaxial Films for GaAs Field Effect Transistors," J. Electrochem Soc. 120, 541, (1973).
4. Private Communication, D. C. Reynolds, PW Yu, AFWAL/AADR, 1981.
5. P. W. Yu, "Iron in Heat Treated Gallium Arsenide," J. Appl. Phys., 52, 5786 (1981).
6. R. D. Fairman, et al, "High Resistivity Chromium Doped GaAs Buffer Layers Grown by Halide Transport Techniques," IEEE Conf. on Active Microwave Devices and Circuits, Cornell Univ., Aug 1979.
7. J. R. Oliver et al, "Undoped Semi-Insulating LEC GaAs: A Model and a Mechanism," Electron Lett. 17, 839 (1981).
8. H. M. Cox and J. V. Di Lorengo, "Review of Techniques for Epitaxial Growth of High Resistivity GaAs," Shiva Ltd., 41 (1980).
9. K. Nakai, et al, "Growth of Iron-Doped Epitaxial Layers for GaAs Field Effect Transistors," J. Electrochem Soc. 124, 1635 (1971).
10. B. I. Boltaks et al, "Diffusion and Solubility of Fe in GaAs," Neorganicheskie Materialy 11, 348 (1975).
11. A. A. Immorlica, et al, "The Effect of Materials Properties on the RF Performance of GaAs FET's Inst. Phys. Soc. 56,423 (1980).
12. P. W. Yu, Private Communication (1982).
13. R. W. Haisty and G. R. Cronin, "A Comparison of Doping Effects of Transitional Elements in Gallium Arsenide," Proc. Int. Conf. on Phy. Semicond., Paris, 1161 (1964).
14. H. Strack, "Electroluminescence of Iron-Sulphur Diffused GaAs Junctions," Trans. Met. Soc. AIME, 239, 381 (1967).



15. P. L. Hoyt and R. W. Haisty, "The Preparation of Epitaxial Semi-Insulating Gallium Arsenide by Iron Doping," J. Electrochem. Soc. 113, 296 (1966).
16. J. Blanc and L. R. Weisberg, "Energy Level Model for High Resistivity Gallium Arsenide," Nature 192, 155 (1961).
17. R. W. Haisty, et al, "Preparation and Characterization of High Resistivity GaAs," J. Phys. Chem. Sol., 23, 829 (1962).
18. J. F. Woods and N. B. Anislie, "Role of Oxygen in Reducing Silicon Contamination of GaAs During Crystal Growth," J. Appl. Phys. 34, 1469, (1963).
19. R. W. Haisty and G. R. Cronin, "Comparison of Doping Effects of Transition Elements in Gallium Arsenide," Proc. 7th Intl. Conf. Semicond. Paris, Academic Press, (1964).
20. J. M. Woodall and J. F. Woods, "Preparation of $0.5-10^3 \Omega \text{ cm}$ GaAs by Acceptor Precipitation During Heat Treatment of Oxygen Grown Crystals," Solid State Comm. 4, 33 (1966).
21. L. Palm, et al, "Effect of Oxygen Injection During VPE Growth of GaAs Films," J. Electronic Mat. 8, 555 (1979).
22. H. C. Casey, et al, "Investigation of Heterojunctions for MIS Devices with Oxygen Doped $\text{Al}_x\text{Ga}_{1-x}\text{As}$ on n Type GaAs," J. Appl. Phys. 50, 3484 (1979).
23. SIMS analysis contracted to Charles Evans and Associates, San Mateo, California.
24. D. W. Kisker, et al, "Oxygen Gettering by Graphite Baffles During Organometallic Vapor Phase Epitaxial Growth," Appl. Phy. Lett. 40, 614 (1982).
25. P. S. Nayar and C. M. Penchia, "Deep Level Studies of Oxygen Doped GaAs-Au Schottky Barrier Diodes," J. Electron. Matl. 11, 321 (1982).
26. S. R. Mc Afee, et al, "Observation of Deep Level Associated with the GaAs/ $\text{Al}_x\text{Ga}_{1-x}\text{As}$ Interface Grown by Molecular Beam Epitaxy," Appl. Phy Lett. 40, 520 (1982).
27. M. Taniguchi, et al, "Oxygen-Related Deep Level and the Annealing Behavior in GaAs," Proc. 2nd Semi-Insulating Materials Conf., Evian, France, (1982).



Rockwell International

MRDC41086.2ARF

28. C. N. Cochran and L. M. Foster, "Reactions of Gallium with Quartz and with Water Vapor with Implications in the Synthesis of GaAs," J. Electrochem. Soc., 109, 149 (1962).
29. H. Fukui, et al, "Reliability of Power GaAs Field-Effect Transistors," IEEE Trans. on Electron. Dev. ED-29, 395 (1982).